ARTICLES
https://doi.org/10.1038/s41591-020-0805-8

nature medicine

Check for updates

Neoadjuvant immunotherapy leads to pathological responses in MMR-proficient and MMR-deficient early-stage colon cancers

Myriam Chalabi[1,2,3]✉, Lorenzo F. Fanchi[2,4,17], Krijn K. Dijkstra[2,4,17], José G. Van den Berg[5,17], Arend G. Aalbers[6], Karolina Sikorska[7], Marta Lopez-Yurda[7,8], Cecile Grootscholten[1], Geerard L. Beets[6,9], Petur Snaebjornsson[5], Monique Maas[10], Marjolijn Mertz[11], Vivien Veninga[2,4], Gergana Bounova[4,12], Annegien Broeks[13], Regina G. Beets-Tan[9,10], Thomas R. de Wijkerslooth[1], Anja U. van Lent[14], Hendrik A. Marsman[15], Elvira Nuijten[7], Niels F. Kok[6], Maria Kuiper[1], Wieke H. Verbeek[1], Marleen Kok[3,16], Monique E. Van Leerdam[1], Ton N. Schumacher[2,4], Emile E. Voest[1,2,4,17]✉ and John B. Haanen[2,3,17]

PD-1 plus CTLA-4 blockade is highly effective in advanced-stage, mismatch repair (MMR)-deficient (dMMR) colorectal cancers, yet not in MMR-proficient (pMMR) tumors. We postulated a higher efficacy of neoadjuvant immunotherapy in early-stage colon cancers. In the exploratory NICHE study (ClinicalTrials.gov: NCT03026140), patients with dMMR or pMMR tumors received a single dose of ipilimumab and two doses of nivolumab before surgery, the pMMR group with or without celecoxib. The primary objective was safety and feasibility; 40 patients with 21 dMMR and 20 pMMR tumors were treated, and 3 patients received nivolumab monotherapy in the safety run-in. Treatment was well tolerated and all patients underwent radical resections without delays, meeting the primary endpoint. Of the patients who received ipilimumab + nivolumab (20 dMMR and 15 pMMR tumors), 35 were evaluable for efficacy and translational endpoints. Pathological response was observed in 20/20 (100%; 95% exact confidence interval (CI): 86–100%) dMMR tumors, with 19 major pathological responses (MPRs, ≤10% residual viable tumor) and 12 pathological complete responses. In pMMR tumors, 4/15 (27%; 95% exact CI: 8–55%) showed pathological responses, with 3 MPRs and 1 partial response. CD8$^+$PD-1$^+$ T cell infiltration was predictive of response in pMMR tumors. These data indicate that neoadjuvant immunotherapy may have the potential to become the standard of care for a defined group of colon cancer patients when validated in larger studies with at least 3 years of disease-free survival data.

Immune checkpoint inhibition (ICI) directed against programmed death-1 (PD-1) and cytotoxic T lymphocyte antigen-4 (CTLA-4) proteins is highly effective and has become the standard of care for patients with dMMR metastatic colorectal cancers (mCRCs). In contrast, the same regimens have shown poor response rates in patients with metastatic pMMR mCRCs. This differential outcome has been attributed to the higher mutational burden of dMMR tumors, particularly the accumulation of insertions–deletions (indels), giving rise to more neoantigens[1–5]. Possibly as a result of their higher neoantigen burden, dMMR tumors are also characterized by an increased density of intratumoral T cells[6,7]. Although no data are available on colon cancers (CCs), in several tumor types an increased T cell infiltration (TCI) has been shown to increase the probability of response to ICI[8,9].

Recent studies in early-stage melanoma, lung cancer and bladder cancer have shown impressive and deep pathological responses to neoadjuvant ICI[10–14]. The higher response rates in early-stage disease compared with metastatic disease have been attributed to a difference in TCI, a lower degree of systemic immune suppression, the absence of visceral metastases and a lower tumor burden[10,14]. Interestingly, in early-stage pMMR CCs, a substantial proportion of tumors has a high TCI compared with metastatic pMMR CCs[6,15], and this prompted us to investigate the activity of neoadjuvant ICI in both dMMR and pMMR early-stage CCs. As the vast majority of pMMR mCRC patients do not benefit from ICI, we combined ICI with the cyclooxygenase (COX)-2 inhibitor celecoxib. This is based on preclinical data suggesting that prostaglandin E_2 (PGE_2) leads to subversion of myeloid cells and increases tumor-promoting

[1]Gastrointestinal Oncology, Netherlands Cancer Institute, Amsterdam, the Netherlands. [2]Molecular Oncology and Immunology, Netherlands Cancer Institute, Amsterdam, the Netherlands. [3]Medical Oncology, Netherlands Cancer Institute, Amsterdam, the Netherlands. [4]Oncode Institute, Utrecht, the Netherlands. [5]Pathology, Netherlands Cancer Institute, Amsterdam, the Netherlands. [6]Surgical Oncology, Netherlands Cancer Institute, Amsterdam, the Netherlands. [7]Biometrics, Netherlands Cancer Institute, Amsterdam, the Netherlands. [8]Princess Máxima Center for Pediatric Oncology, Utrecht, the Netherlands. [9]GROW School for Oncology and Developmental Biology, Maastricht University, Maastricht, the Netherlands. [10]Radiology, Netherlands Cancer Institute, Amsterdam, the Netherlands. [11]Bioimaging Facility, Netherlands Cancer Institute, Amsterdam, the Netherlands. [12]Molecular Carcinogenesis, Netherlands Cancer Institute, Amsterdam, the Netherlands. [13]Core Facility Molecular Pathology & Biobanking, Netherlands Cancer Institute, Amsterdam, the Netherlands. [14]Gastroenterology & Hepatology, Onze Lieve Vrouwe Gasthuis, Amsterdam, the Netherlands. [15]Surgery, Onze Lieve Vrouwe Gasthuis, Amsterdam, the Netherlands. [16]Tumor Biology & Immunology, Netherlands Cancer Institute, Amsterdam, the Netherlands. [17]These authors contributed equally: Lorenzo F. Fanchi, Krijn K. Dijkstra, José G. Van den Berg, Emile E. Voest, John B. Haanen. ✉e-mail: m.chalabi@nki.nl; e.voest@nki.nl

Table 1 | Baseline patient characteristics according to MMR status ($n = 40$)

	dMMR tumors ($n = 21$)	pMMR tumors ($n = 19$)
Age at enrollment (years)		
Median (range)	58.4 (22–82)	65.9 (44–77)
Sex (*n* (%))		
Female	12 (57)	10 (53)
Male	9 (43)	9 (47)
Eastern Cooperative Oncology Group performance status		
0	21 (100)	19 (100)
Clinical disease stage (*n* (%))		
I	2 (9.5)	5 (20)
II	2 (9.5)	7 (35)
IIIA	1 (4.8)	1 (5)
IIIB	10 (47.6)	6 (30)
IIIC	6 (28.6)	1 (5)
Primary tumor location (*n* (%))		
Right colon	14 (67)	8 (42)
Left colon	5 (24)	11 (58)
Transverse colon	2 (10)	1 (5)
Lynch syndrome	7 (33)	0 (0)

Percentages may not total 100 because of rounding. One patient with both a dMMR and a pMMR tumor is accounted for once in the patient characteristics of the dMMR group, and separately per tumor for the tumor-specific features, making a total of 21 dMMR and 20 pMMR tumors.

inflammation. In turn, inhibition of PGE_2 synthesis by COX-2 inhibition may have synergistic effects with ICI[16].

In the present study, we report the first results from the ongoing exploratory NICHE study, investigating the safety, feasibility, activity and immunological correlates of short-term, preoperative ipilimumab/nivolumab with or without celecoxib in patients with nonmetastatic CCs.

In the NICHE study (NCT03026140), patients received combination treatment with ipilimumab ($1\,mg\,kg^{-1}$) on day (D) 1 + nivolumab ($3\,mg\,kg^{-1}$) on D1 and D15, and patients with pMMR tumors were randomly assigned to receive celecoxib from D1 until the day before surgery, in addition to ICI. Pretreatment tumor biopsies were taken during colonoscopies and posttreatment tissue was obtained at surgery. Surgery was performed a maximum of 6 weeks after inclusion (see Extended Data Fig. 1). The primary objective was safety and feasibility. Secondary objectives included efficacy, which was assessed by histopathological response and changes in T cell infiltrates. MPR was defined as ≤10% of residual viable tumor in the surgical specimen (see Methods)[14,17,18].

Results

Patient characteristics. Forty patients were treated, with a total of 21 dMMR and 20 pMMR tumors (one patient had both a pMMR and a dMMR CC). The first patient was enrolled on 29 March 2017. By pretreatment radiological assessment, 81% of patients with dMMR tumors and 40% with pMMR tumors had clinical stage III disease. Baseline patient characteristics are shown in Table 1. After a safety run-in of 3 patients who received nivolumab monotherapy, 37 patients were treated with ipilimumab + nivolumab. Of 17 patients in the pMMR group, 8 were randomized to receive celecoxib. Two patients with pMMR tumors who did not meet inclusion criteria (liver metastases at baseline, and mixed adenocarcinoma and neuroendocrine carcinoma, both confirmed after neoadjuvant treatment and surgery) were excluded from efficacy and subsequent analyses, leaving 15 patients with pMMR (7 with celecoxib) and 20 with dMMR tumors who received ipilimumab + nivolumab, who are evaluable for efficacy and translational endpoints (see Extended Data Fig. 2).

Safety. Treatment was well tolerated and all patients underwent radical resections within the predefined 6 weeks after study inclusion, with primary anastomoses in all patients. Of the resections 100% were radical. The median duration from the first dose of nivolumab to surgery was 32 d (interquartile range (IQR) 30, 34 d). Five patients (13%) experienced grade 3–4 treatment-related toxicity (see Supplementary Table 1). Two patients experienced a grade 3 rash, which resolved on steroid treatment (one oral, one topical); one patient experienced a grade 3 colitis 2 months after surgery, for which a single dose of infliximab was given with resolution of symptoms within 3 d. The three remaining grade 3–4 adverse events (AEs) were asymptomatic increases in laboratory tests, which resolved spontaneously.

Surgery-related, grade 3 AEs were observed in eight patients (see Supplementary Table 2). Anastomotic leakage was observed in 4 of 40 (10%, 95% CI 3–24%) patients. One patient with a pathological complete response (pCR) of a dMMR tumor had signs of colitis on histopathological assessment, which was asymptomatic and most probably secondary to response. In the other three patients, no evidence of colitis or other relationship of the anastomotic leak to neoadjuvant treatment was found.

Neoadjuvant ipilimumab + nivolumab leads to pathological responses in MMR-deficient and -proficient tumors. All (20/20, 100% (95% exact CI: 86–100%)) patients with dMMR tumors had a pathological response. Nineteen patients had an MPR with ≤10% residual viable tumor, and this included 12 (60%; 95% exact CI 36–81%) pCRs (Fig. 1). Nine of the twelve dMMR tumors with pCRs were clinical stage III before treatment (see Supplementary Table 3). One patient with 18% residual viable tumor was classified as a partial responder. In addition, and in contrast to the lack of responses seen in metastatic pMMR tumors, 4/15 (27%, 95% exact CI 8–55%) patients with pMMR tumors, who received combination treatment with ipilimumab + nivolumab, showed a pathological response. Three of these pMMR responders had an MPR, with two pCRs and one tumor with 1% residual viable tumor (Fig. 1, and see Supplementary Table 4). The fourth patient showed a partial response (PR) with 50% residual viable tumor. In addition, four other patients had evidence of response, varying from 60% to 85% of residual viable tumor (Fig. 1, and see Supplementary Table 4). Of the seven patients with a pMMR tumor who received celecoxib in addition to ipilimumab + nivolumab, two showed a response (one MPR and one PR) and two other patients had tumor regression of 10–50%.

Three patients with pMMR tumors, and one patient with a dMMR tumor (with a PR) and positive lymph nodes after surgery, received adjuvant chemotherapy. Two elderly patients (aged 76 and 78 years) with dMMR tumors and positive lymph nodes did not receive adjuvant chemotherapy after consideration of the lack of benefit of oxaliplatin in patients aged >70 years and the inefficacy of adjuvant treatment with 5-fluorouracil/capecitabine monotherapy in dMMR tumors, in accordance with national guidelines. Median follow-up at data cut-off was 9 months (IQR 5.3–15.7 months), 8.1 months for the dMMR subgroup (range 5.6–13.8 months) and 9.8 months for the pMMR subgroup (range 4.2–22.1 months). All patients with dMMR tumors were alive and disease free at data cut-off. Of the patients with pMMR tumors, one had died (disease-unrelated cardiovascular event) and one with a pT3N1 tumor, without pathological response after ICI, developed a liver metastasis and underwent metastasectomy. This patient later also developed

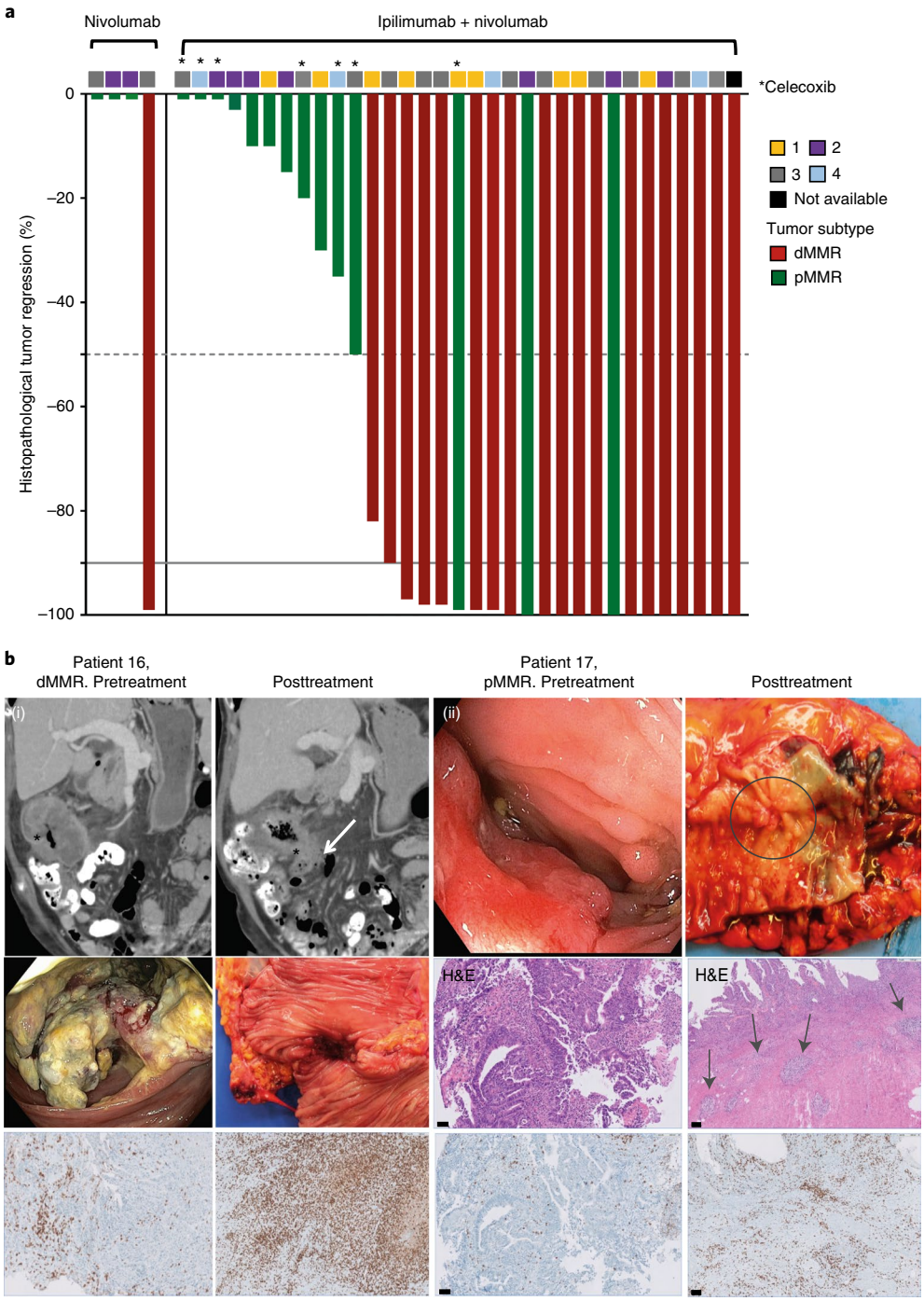

Fig. 1 | Pathological response after neoadjuvant ICI. a, Percentage pathological regression shown per tumor. The gray horizontal line depicts the demarcation for MPRs corresponding to 90% regression. The dotted line demarcates PR (50% regression). The vertical black line separates patients treated with nivolumab monotherapy in the run-in part of the study (left) and combination ipilimumab + nivolumab (right). Asterisks depict pMMR patients who received celecoxib. Upper bar: CMS subtyping per tumor. **b**, Radiological and pathological response to neoadjuvant therapy with ipilimumab, nivolumab and celecoxib. (i) Top left: CT imaging of the abdomen of an 82-year-old woman with stage IIIc/cT4aN2a, right-sided, dMMR CC before treatment. The primary tumor (*) is shown in the hepatic flexure with hypodense compartments suggestive of mucinous or necrotic areas. Top right: posttreatment CT scan showed notable decrease in tumor volume, and yet increased tumor invasion in the small bowel (arrow) with a more solid aspect of the tumor, rendering posttreatment radiological staging ycT4bN2a. Histopathological evaluation of the resection specimen revealed a CR of both the primary tumor and the lymph nodes. Middle row: pre- and posttreatment pictures of the tumor. Bottom: CD8 staining on pre- (left) and posttreatment (right) samples. (ii) Top left: endoscopic picture of a sigmoid pMMR CC, stage IIa/cT3N0 in a 77-year-old woman. Top right: posttreatment resection specimen with mucosal retraction at the site of tumor location and a polypoid structure. Middle left: pretreatment biopsy showing an intestinal-type adenocarcinoma with a variable dense infiltrate (H&E staining). Middle right: posttreatment H&E stain showing fields of high-grade dysplasia (top of the images) and complete regression of the invasive adenocarcinoma. In the submucosa, fibrosis and an infiltrate with variable density with many TLSs (arrowheads) are shown. Bottom: CD8 staining pre- (left) and posttreatment (right). This patient did not receive celecoxib.

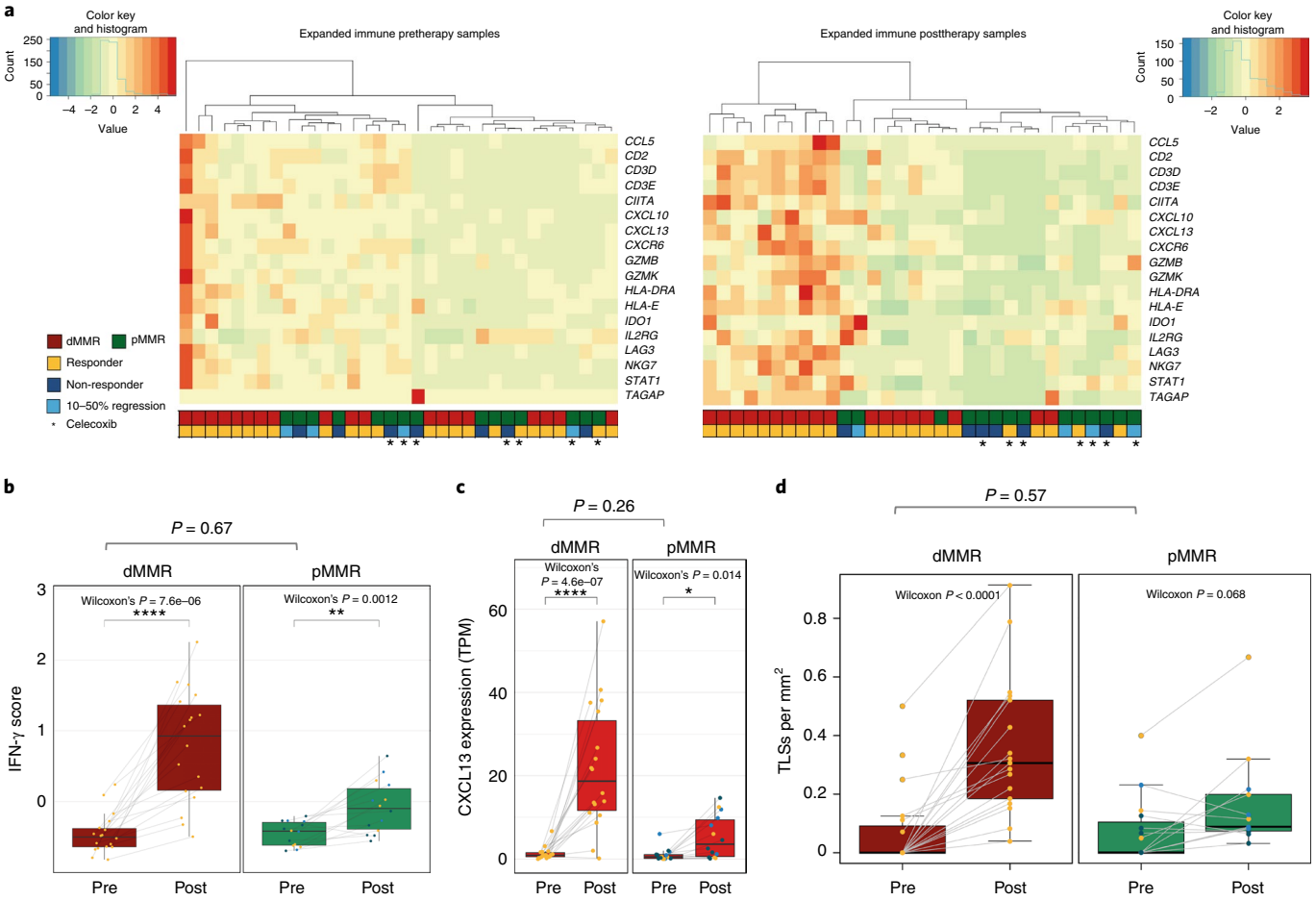

Fig. 2 | Immune gene signatures, IFN-γ score and TLSs in predicting response to checkpoint blockade. a, Unsupervised clustering of immune-related genes (Ayers et al.[33]) per tumor according to MMR status and response: pretreatment (left) and, posttreatment (right) samples. **b**, Pre- to posttreatment changes in IFN-γ score according to MMR status and response. Pretreatment comparison of IFN-γ score between dMMR (left, $n=18$) and pMMR (right, $n=14$) tumors are shown at the top of the figure. Responders are depicted in yellow and nonresponders in dark blue, and tumors with 10–50% regression in light blue. Boxplots represent the median, and 25th and 75th percentiles; the whiskers extend from the hinge to the largest value no further than 1.5× IQR from the hinge. Pre- to postpairwise statistical significance was tested using Wilcoxon's signed-rank test; for differences between pMMR and dMMR tumors, the significance was tested using Wilcoxon's rank-sum test. All statistical tests were two sided. **c**, Single-gene expression of CXCL13, shown in TPM, pre- to posttreatment in dMMR (left, $n=18$) and pMMR (right, $n=14$) tumors. Boxplots represent the median, and 25th and 75th percentiles; the whiskers extend from the hinge to the largest value no further than 1.5× IQR from the hinge. Pre- to postpairwise statistical significance was tested using Wilcoxon's signed-rank test; for differences between pMMR and dMMR tumors, the significance was tested using Wilcoxon's rank-sum test. All statistical tests were two sided. **d**, Changes in numbers of TLSs, defined as CD20$^+$ lymphoid aggregates (≥100 lymphocytes) with a germinal center, pre- to posttreatment in dMMR (left, $n=18$) and pMMR (right, $n=13$) tumors. Boxplots represent the median, and 25th and 75th percentiles; the whiskers extend from the hinge to the largest value no further than 1.5× IQR from the hinge. Pre- to postpairwise statistical significance was tested using Wilcoxon's signed-rank test; for differences between pMMR and dMMR tumors, the significance was tested using Wilcoxon's rank-sum test. All statistical tests were two sided. **b**–**d**, No adjustments were made for multiple comparisons.

peritoneal metastases and underwent palliative systemic therapy. All other patients were alive and disease free.

The tumor regression observed in most patients was characterized by a mixed inflammatory infiltrate, fibrous tissue, pools of acellular mucin and, in four dMMR and one pMMR tumors, areas of necrosis surrounded by histiocytic infiltration. The mucosal surface was often ulcerated and replaced by granulation tissue. The submucosa showed scarring and variable neuronal hyperplasia. Four pMMR tumors with 65–85% residual viable tumor in the resection specimen did show fibrosis and inflammation similar to that found in the four tumors from pMMR responders, but were classified and analyzed as nonresponders (Fig. 1, and see Supplementary Table 4). In evaluable patients receiving ipilimumab + nivolumab, all tumors (both dMMR and pMMR) harbored tertiary lymphoid structures (TLSs) at the time of resection. TLSs have been associated with an improved prognosis in many cancer types and found to harbor most PD-1$^+$ tumor-infiltrating lymphocytes (TILs) in lung cancer, which in turn are thought to play a key role in the recruitment of immune subsets to the tumor microenvironment (TME)[17,19]. In the present study, a significant pre- to posttreatment increase in TLSs was found in dMMR tumors ($P<0.0001$), with a nonsignificant trend in pMMR tumors ($P=0.07$; Fig. 2).

Radiological evaluation of treatment response was performed using CT scans before surgery in 14 patients (10 dMMR and 4 pMMR tumors; see Supplementary Tables 3 and 4). Correlation between radiological assessment of response and histopathological findings was poor. In particular, responding patients with an MPR on histopathological assessment were often evaluated as having gross residual disease based on the CT scan (Fig. 1). These results indicate that the current assessment of treatment effect using CT

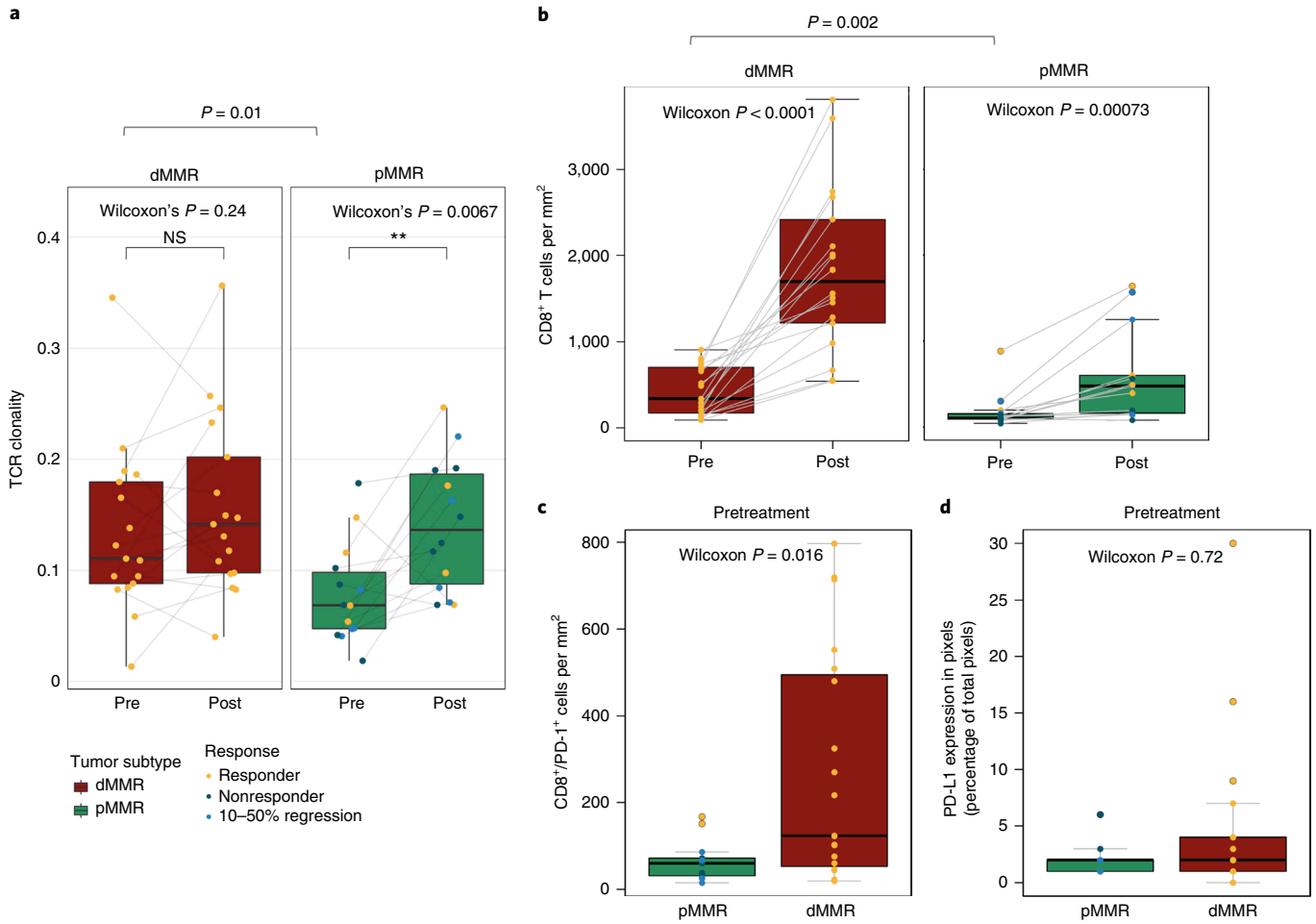

Fig. 3 | TCR clonality, CD8⁺ TCI, T cell phenotyping and PD-L1 expression. a, Pretreatment TCR clonality in dMMR (left, $n=17$) versus pMMR (right, $n=14$) tumors and changes in TCR clonality pre- to posttreatment in pMMR and dMMR tumors. Boxplots represent the median, and 25th and 75th percentiles; the whiskers extend from the hinge to the largest value no further than 1.5× IQR from the hinge. Pre- to postpairwise statistical significance was tested using Wilcoxon's signed-rank test; for differences between pMMR and dMMR tumors, the significance was tested using Wilcoxon's rank-sum test. All statistical tests were two sided. **b**, Pre- to posttreatment changes in CD8⁺ TCI in dMMR (left, $n=19$) and pMMR (right, $n=15$) tumors. Boxplots represent the median, and 25th and 75th percentiles; the whiskers extend from the hinge to the largest value no further than 1.5× IQR from the hinge. Pre- to postpairwise statistical significance was tested using Wilcoxon's signed-rank test; for differences between pMMR and dMMR tumors, the significance was tested using Wilcoxon's rank-sum test. All statistical tests were two sided. **c**, Pretreatment, CD8⁺PD-1⁺ double-positive T cells in pMMR (left, $n=13$) versus dMMR (right, $n=19$) tumors, using double staining for CD8 and PD-1. Boxplots represent the median, and 25th and 75th percentiles; the whiskers extend from the hinge to the largest value no further than 1.5× IQR from the hinge. The significance for differences between pMMR and dMMR tumors was tested using Wilcoxon's rank-sum test. Statistical tests were two sided. **d**, PD-L1 expression in pMMR (left, $n=15$) versus dMMR (right, $n=18$) tumors, shown in pixel counts as a percentage of total pixel count. Boxplots represent the median, and 25th and 75th percentiles; the whiskers extend from the hinge to the largest value no further than 1.5× IQR from the hinge. The significance for differences between pMMR and dMMR was tested using Wilcoxon's rank-sum test. Statistical tests were two sided. **a**–**d**, No adjustments were made for multiple comparisons. NS, not significant.

scans vastly underestimates responses in dMMR tumors, and that further research should focus on the development of new imaging biomarkers combined with molecular markers to provide a more accurate assessment, and perhaps prediction, of response to neoadjuvant immunotherapy.

Biomarker analysis of neoadjuvant ICI response in CC. To further assess the impact of the combination ipilimumab + nivolumab on the TME, we performed extensive analyses using whole-exome sequencing, immunohistochemistry (IHC), immune-related gene signatures and T cell receptor (TCR) sequencing. For 13 patients, TCR sequencing was also performed on peripheral blood mononuclear cell (PBMC) samples pre- and posttreatment.

As expected, a profound difference in pretreatment tumor mutational burden (TMB) between dMMR and pMMR tumors was observed, with a median of 1,438 (range 648–4,458) and 111 (range 48–261) mutations, respectively ($P<0.0001$; see Extended Data Fig. 3). Strikingly, responses in pMMR tumors were seen despite a low pretreatment TMB, and TMB was not notably different between pMMR responders and nonresponders (median 108 (IQR 62–153) versus 117 (IQR 93–143); Fig. 4). Recent work has suggested that the formation of neoantigens as a consequence of indels may be of particular importance to tumor control[5]. Notably, the number of indels was not substantially different between pMMR responders and nonresponders (median 5 (IQR 3.3–6.8) versus 4.5 (IQR 2–7.3)), but the number of indels in pMMR responders was remarkably lower than that observed in dMMR responders (median 5 versus 392).

Baseline tumor biopsies revealed a significantly higher CD8⁺ TCI ($P=0.002$), CD68⁺ immune infiltration ($P=0.042$), CD8⁺PD-1⁺

TCI ($P=0.016$) and TCR clonality ($P=0.007$) in dMMR tumors compared with pMMR tumors (Fig. 3, and see Supplementary Fig. 3). In contrast, no notable differences were found at baseline between dMMR and pMMR tumors for CD3$^+$ and FOXP3$^+$ TCI, PD ligand 1 (PD-L1) expression, interferon (IFN)-γ scores, TLS presence or chemokine CXCL13 expression (Fig. 2, and see Extended Data Fig. 3).

Extensive analyses were also performed comparing pMMR responders and pMMR nonresponders to gain insight into drivers of response, or resistance, and find possible pretreatment biomarkers predictive of response (see Extended Data Figs. 3 and 4). Strikingly, the sole biomarker found to predict response in pMMR tumors was the presence of T cells with co-expression of CD8 and PD-1 (CD8$^+$PD-1$^+$ TCI). Other more established pretreatment biomarkers, including TCR clonality, CD3$^+$, CD8$^+$ and FOXP3$^+$ TCI, IFN-γ score, TLS presence and CXCL13 expression, were not notably different between pMMR responders and nonresponders (Fig. 4). The lack of difference in CXCL13 expression and TLS presence at baseline suggests that, in CC, PD-1$^+$ T cells might not be predominantly present in TLS, as was observed in nonsmall-cell lung cancer[19]. Transforming growth factor (TGF)-β signatures were numerically higher in pretreatment samples of nonresponders, although the difference was not notable. TGF-β signatures have been associated with nonresponse to ICI in bladder cancer and preclinical models of CRCs, and in these preclinical models improved responses to ICI are seen when combined with TGF-β inhibition[20,21].

The most established classification system of CRCs based on gene expression is the consensus molecular subtype (CSM) subtyping, which has been proposed as a new prognostic tool for CRCs and is increasingly being tested in prospective studies for treatment efficacy[22,23]. In our cohort, pMMR responders did not cluster into a specific subtype (see Fig. 1).

Neoadjuvant ICI induces changes in the CC TME. In posttreatment surgical specimens, dMMR tumors showed significant increases in CD8$^+$ ($P<0.0001$; see Fig. 3) and CD3$^+$ TCI ($P<0.0001$; see Extended Data Fig. 3), as well as IFN-γ scores ($P<0.0001$; see Fig. 2), when compared with pretreatment biopsies, in agreement with the MPRs observed in these tumors. A significant increase in TLS presence ($P<0.0001$) and CXCL13 expression ($P<0.0001$) was also observed in these tumors (see Fig. 2). Despite the responses seen, TCR clonality did not increase notably in dMMR tumors posttreatment, which is probably due to the high TCR clonality found in these tumors pretreatment (see Fig. 3). There was a nonsignificant trend for increased CD68$^+$ immune infiltration ($P=0.07$; see Extended Data Fig. 3).

Assessment of posttreatment changes in pMMR tumors revealed a significant increase in CD8$^+$ TCI ($P<0.0001$; see Fig. 3) and CD68$^+$ immune infiltration ($P=0.03$; see Extended Data Fig. 3). In addition, significant posttreatment increases in IFN-γ score ($P=0.001$), TCR clonality ($P=0.007$) and CXCL13 expression ($P=0.01$) were observed in pMMR tumors (see Figs. 2 and 3). Interestingly, assessment of pre- to posttreatment changes in pMMR nonresponders also showed significant increases in CD8$^+$ TCI ($P=0.01$), TCR clonality ($P=0.01$), IFN-γ score ($P=0.02$) and CXCL13 expression ($P=0.04$) in these tumors, indicating that the changes seen in pMMR tumors are not only driven by pMMR responders (Fig. 4). Together, these data suggest that neoadjuvant ICI in

Fig. 4 | Comparisons between pMMR responders and nonresponders for subsets of infiltrating T cells, TCR clonality, CXCL13 expression, IFN-γ score, TMB and TGF-β signatures. a, Pre- to posttreatment changes in TCR clonality in pMMR responders (R, left, $n=4$) versus pMMR nonresponders (NR, right, $n=10$). Boxplots represent the median, and 25th and 75th percentiles; the whiskers extend from the hinge to the largest value no further than 1.5× IQR from the hinge. Pre- to postpairwise statistical significance was tested using Wilcoxon's signed-rank test; for differences between responders and nonresponders, the significance was tested using Wilcoxon's rank-sum test. All statistical tests were two sided. **b**, Pre- to posttreatment changes in CD8$^+$ TCI in pMMR responders (left, $n=4$) and nonresponders (right, $n=9$). Boxplots represent the median, and 25th and 75th percentiles; the whiskers extend from the hinge to the largest value no further than 1.5× IQR from the hinge. Pre- to postpairwise statistical significance was tested using Wilcoxon's signed-rank test; for differences between responders and nonresponders, the significance was tested using Wilcoxon's rank-sum test. All statistical tests were two sided. **c**, Pretreatment infiltration of CD8$^+$PD-1$^+$ double-positive T cells in pMMR responders (left, $n=3$) and nonresponders (right, $n=9$), using double staining for CD8 and PD-1. Boxplots represent the median, and 25th and 75th percentiles; the whiskers extend from the hinge to the largest value no further than 1.5× IQR from the hinge. For pretreatment differences between responders and nonresponders, the significance was tested using Wilcoxon's rank-sum test. All statistical tests were two sided. **d**, Changes in IFN-γ score in pMMR responders (left, $n=4$) and nonresponders (right, $n=10$). Boxplots represent the median, and 25th and 75th percentiles; the whiskers extend from the hinge to the largest value no further than 1.5× IQR from the hinge. Pre- to postpairwise statistical significance was tested using Wilcoxon's signed-rank test; for differences between responders and nonresponders, the significance was tested using Wilcoxon's rank-sum test. All statistical tests were two sided. **e**, Pre- to posttreatment changes in numbers of TLSs, detected using CD20-stained slides in responders (left) and nonresponders (right). Boxplots represent the median, and 25th and 75th percentiles; the whiskers extend from the hinge to the largest value no further than 1.5× IQR from the hinge. Pre- to postpairwise statistical significance was tested using Wilcoxon's signed-rank test; for differences between responders and nonresponders, the significance was tested using Wilcoxon's rank-sum test. All statistical tests were two sided. **f**, Pre- to posttreatment changes in CXCL13 expression in pMMR responders (left, $n=4$) and nonresponders (right, $n=10$). Boxplots represent the median, and 25th and 75th percentiles; the whiskers extend from the hinge to the largest value no further than 1.5× IQR from the hinge. Pre- to postpairwise statistical significance was tested using Wilcoxon's signed-rank test; for differences between responders and nonresponders, the significance was tested using Wilcoxon's rank-sum test. All statistical tests were two sided. **g**, Pre- to posttreatment changes in CD3$^+$ TCI in pMMR responders (left, $n=4$) and nonresponders (right, $n=9$). Boxplots represent the median, and 25th and 75th percentiles; the whiskers extend from the hinge to the largest value no further than 1.5× IQR from the hinge. Pre- to postpairwise statistical significance was tested using Wilcoxon's signed-rank test; for differences between responders and nonresponders, the significance was tested using Wilcoxon's rank-sum test. All statistical tests were two sided. **h**, FOXP3$^+$ TCI in pMMR responders (left, $n=4$) and nonresponders (right, $n=9$). Boxplots represent the median, and 25th and 75th percentiles; the whiskers extend from the hinge to the largest value no further than 1.5× IQR from the hinge. Pre- to postpairwise statistical significance was tested using Wilcoxon's signed-rank test; for differences between responders and nonresponders, the significance was tested using Wilcoxon's rank-sum test. All statistical tests were two sided. **i**, TMB in pMMR responders (left, $n=4$) and nonresponders (right, $n=10$). Boxplots represent the median, and 25th and 75th percentiles; the whiskers extend from the hinge to the largest value no further than 1.5× IQR from the hinge. For differences between responders and nonresponders, the significance was tested using Wilcoxon's rank-sum test. All statistical tests were two sided. **j**, Pretreatment expression of TGF-β-induced genes at baseline for pMMR responders (left columns, $n=4$) versus nonresponders (right columns, $n=10$) (fibroblast TGF-β-responsive signature (FTBRS) and T cell–TBRS (TTBRS)). Boxplots represent the median, and 25th and 75th percentiles; the whiskers extends from the hinge to the largest value no further than 1.5× IQR from the hinge. For pretreatment differences between responders and nonresponders, the significance was tested using Wilcoxon's rank-sum test. All statistical tests were two sided. **a**–**j**, No adjustments were made for multiple comparisons.

early-stage pMMR CCs commonly leads to immune activation, even when this does not culminate in a pathological response in all patients.

To test whether the expansion of TCRs found in tissue could be detected systemically, we performed TCR sequencing on pre- and posttreatment blood for 13 patients (14 tumors total due to one

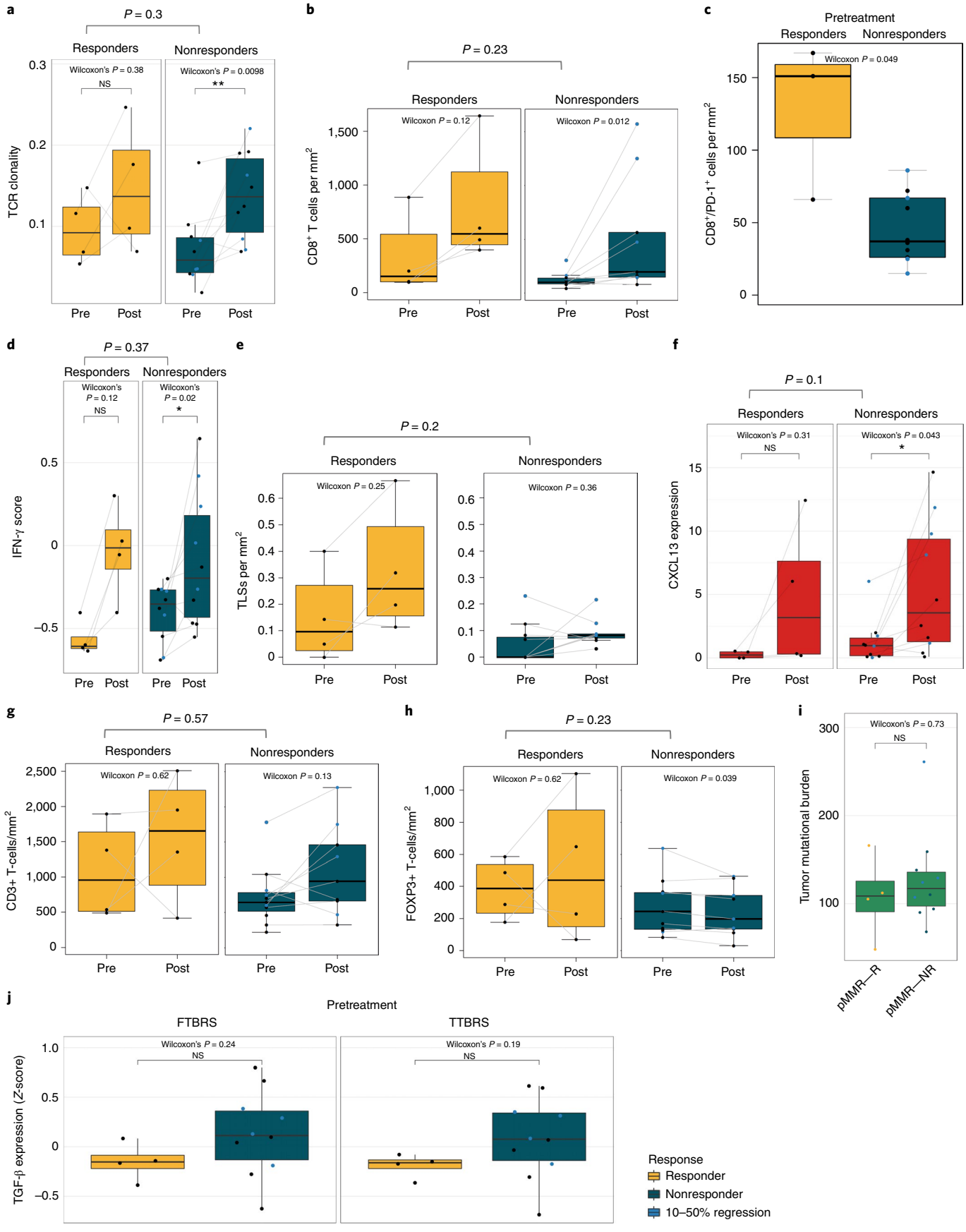

patient having a double tumor, yielding 3 pMMR responders, 5 pMMR nonresponders and 6 dMMR responders; see Extended Data Fig. 5). Patients with a pathological response did not have a higher frequency of T cell clones that were shared between tissue and blood (neither pMMR nor dMMR), when compared with pMMR nonresponders. As shown above, no differences were found when analyzing tissue-resident TCRs only (see Extended Data Fig. 3). In all patients tested, posttreatment peripheral expansion of multiple shared T cell clones between tissue and blood was observed. Some of these clones were not detectable pretreatment (see Extended Data Fig. 5).

CC organoids derived from clinical responders can be recognized by autologous T cells. Using a recently developed platform of co-cultures between tumor organoids and autologous T cells[24], we established organoids from six pMMR nonresponders, one pMMR partial responder (30% regression) and five dMMR responders. Organoids were then co-cultured, in the presence of PD-1-blocking antibodies, with peripheral blood lymphocytes (PBLs) obtained after ICI treatment[24]. After 2 weeks of co-culture, no reactivity was observed in pMMR nonresponders. In contrast, reactivity was seen for three of six responders (Fig. 5a,b, and see Extended Data Fig. 4), including the pMMR tumor with a PR. For one dMMR responder, absence of in vitro $CD8^+$ T cell reactivity was explained by lack of major histocompatibility complex (MHC)-I expression on organoids (see Extended Data Fig. 4). In general, there was no difference in MHC-I expression level between pMMR and dMMR organoids (see Extended Data Fig. 4), indicating that the lack of response in pMMR organoids was not a result of MHC-I loss.

One patient (N3) presented with a synchronous dMMR (responding) and a pMMR (nonresponding) tumor. Organoids were established from both tumors, and co-cultures of PBLs and organoids induced T cell reactivity only against the dMMR tumor (Fig. 5c,d). Similar to PBLs, tumor reactivity of TILs was restricted to organoids derived from the dMMR tumor (Fig. 5c,d). For three responders who showed in vitro tumor reactivity using posttreatment T cells, we also performed co-cultures of organoids and pretreatment PBLs. Tumor reactivity could be induced using pretreatment PBLs for the dMMR tumor with a complete response, but not for the pMMR tumor with a PR (N26) (see Extended Data Fig. 4). For the third patient (N3), tumor reactivity of pretreatment PBLs has been described previously[24].

To test whether lack of response in pMMR tumors may be explained by a lack of tumor antigens or by other tumor-intrinsic factors, co-culture experiments were performed using a matched antigen–TCR system (see Methods). Melanoma-associated antigen MART-1[25] was loaded on human leukocyte antigen (HLA)-A2-transduced pMMR and dMMR tumor organoids (see Extended Data Fig. 4). MART-1-specific 1D3 TCR T cells stimulated with these organoids resulted in similar IFN-γ secretion for pMMR and dMMR organoids (Fig. 5e). These data do not provide evidence for a tumor-intrinsic factor directly hampering T cell reactivity in pMMR tumors, and suggest that a major impediment to T cell reactivity in pMMR tumors is the lack of strong T cell antigens.

The organoid co-culture data presented here suggest that T cell reactivity on co-culture of tumor organoids and PBLs is restricted to tumors showing clinical response to ICI, and that, even though ICI leads to immune activation in pMMR nonresponders (see Fig. 4), this is insufficient to induce a population of circulating T cells that can recognize tumor organoids. In vitro reactivity is not observed for all clinical responders, and based on these data this platform may not be best used as a predictor of response to combination PD-1 and CTLA-4 blockade, but could be a tool to gain insight into mechanisms of resistance and ways to overcome resistance.

Discussion

In the present study, we show that neoadjuvant treatment of early-stage CCs with a single dose of ipilimumab and two doses of nivolumab leads to a striking 100% and 27% pathological response in dMMR and pMMR tumors, respectively, after only ~4 weeks of treatment. This treatment is both safe and feasible, with few treatment-related AEs and without compromising surgery.

Recent neoadjuvant ICI response data in melanoma, nonsmall-cell lung cancer and bladder cancer suggest that, for tumor types in which activity is seen in stage IV disease, response rates go up when moving to earlier-stage disease[10–14]. Compared with adjuvant treatment, neoadjuvant ICI has been shown to induce a stronger and broader tumor-specific T cell response[10,26]. The current data demonstrate that ICI can also show activity during early-stage disease in a tumor subtype that was thus far considered nonresponsive to ICI. The observation that early-stage cancers appear more responsive to ICI may be related to a lower level of immunosuppressive host and tumor-intrinsic factors in early-stage disease[27]. Previous studies with neoadjuvant ipilimumab + nivolumab in melanoma have highlighted the power of neoadjuvant immunotherapy, some at the expense of high (70–90%) rates of grade 3–4 toxicity[10,11]. In our study, combination ipilimumab + nivolumab was very well tolerated, with 13% grade 3–4 immune-related AEs. The most evident reasons for this limited toxicity are the low and single dose of ipilimumab (1 mg kg^{-1}) and the shorter duration of treatment.

Data on neoadjuvant chemotherapy in CCs are scarce. In the phase III FOXTROT trial, which evaluated the efficacy of neoadjuvant chemotherapy with locally advanced CCs, 95% of patients with dMMR tumors who received neoadjuvant chemotherapy ($n = 106$) showed little or no response, and only 8.1% of patients with pMMR tumors ($n = 592$) had MPRs to neoadjuvant chemotherapy[28]. Furthermore, in the FOXTROT study a trend toward improved survival was found in patients receiving neoadjuvant

Fig. 5 | Recognition of dMMR or pMMR CC organoids by autologous T cells. a, Representative flow cytometry plots of $CD8^+$ T cells tested for tumor reactivity, after 2 weeks of co-culture with autologous CC organoids. Number of biologically independent experiments: patient N12 ($n = 4$), N26 ($n = 2$). **b**, Quantification of IFN-γ production by $CD8^+$ T cells, obtained by 2-week co-culture with autologous tumor organoids, on stimulation with CC organoids. Background (spontaneous IFN-γ production) is subtracted from organoid-induced IFN-γ production. The pMMR nonresponders are indicated in dark blue ($n = 6$), pMMR tumor with 30% regression in light blue ($n = 1$) and dMMR responders in red ($n = 5$). Number of biologically independent experiments: N3 ($n = 3$), N12 ($n = 4$), N38 ($n = 1$), all other samples ($n = 2$). **c**, Representative flow cytometry plots of $CD8^+$ or $CD4^+$ T cells obtained after 2-week co-culture of PBLs and dMMR or pMMR CC organoids from one patient with a double tumor (N3), or expanded TILs from the dMMR or pMMR tumor. T cells were re-stimulated with dMMR (red boxes) or pMMR CC organoids (blue boxes), or left unstimulated, and evaluated for intracellular staining of IFN-γ and cell surface staining of CD107a. The number of biologically independent experiments: PBLs ($n = 3$), TILs ($n = 1$). **d**, Quantification of IFN-γ-positive T cells in response to stimulation with pMMR ($n = 1$) or dMMR ($n = 1$) CC organoids from patient N3. Background (IFN-γ-positive cells in unstimulated condition) was subtracted from the signal. Data for PBLs that were both co-cultured with and tested for reactivity against dMMR organoids, or pMMR organoids, are the same as in **b**. Number of biologically independent experiments: for PBLs ($n = 3$), TILs ($n = 1$, 2 technical replicates). **e**, IFN-γ concentration in supernatant 24 h after stimulation with HLA-A2-transduced pMMR ($n = 2$) or dMMR ($n = 2$) CC organoids, loaded with 0.1 μg ml^{-1} of MART-1 peptide. T cell:target cell ratio = 5:1 ($n = 4$ biologically independent experiments). **b**,**d**,**e**, Dots indicate independent experiments. The horizontal bar indicates mean and the error bar denotes s.e.m.

chemotherapy. Importantly, FOXTROT was the first study to show that pathological response to neoadjuvant treatment in CCs is closely related to recurrence risk, with 0% and 8% recurrences in patients with a pCR and marked regression, respectively, compared with 26% for patients with no regression. Compared with these data, our study shows an impressive pathological response rate after

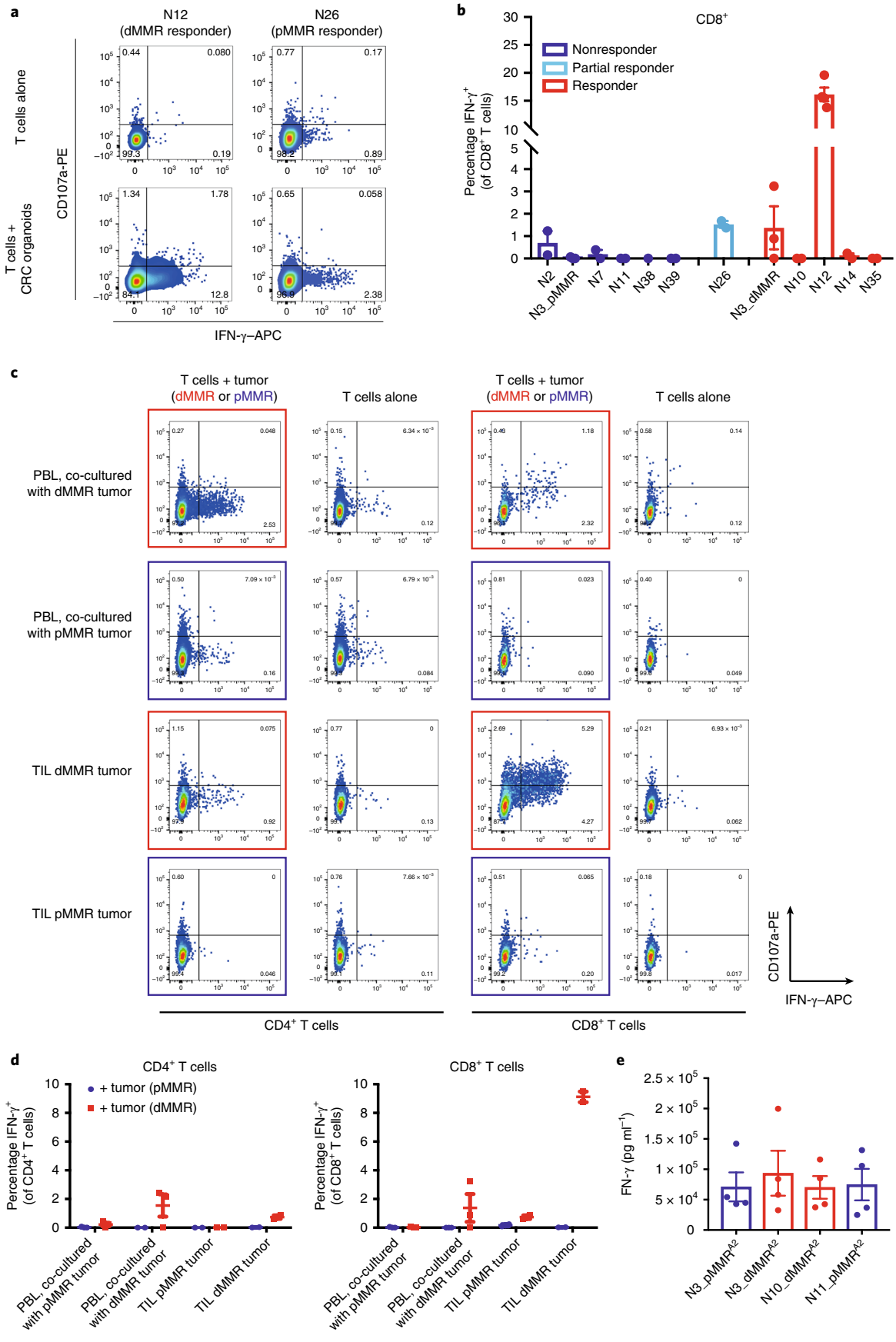

~4 weeks of treatment and may be the first step toward implementation of neoadjuvant immunotherapy in CCs.

Recurrence risk for stage III dMMR and pMMR CCs is similar, and remains high at 25% despite adjuvant chemotherapy and, when N2 disease is considered separately, the recurrence rate is 40% (refs. [29,30]). Neoadjuvant immunotherapy could become the standard of care, but only after larger studies and longer follow-up with at least 3-year, disease-free survival data available, including validation of recent data on the correlation of pathological response with decreased recurrence risk.

In metastatic dMMR CRCs, 55% (65/119) of patients showed objective clinical responses to combination treatment with ipilimumab + nivolumab, with a median time to response of 2.8 months[1]. In contrast, ICI has been largely ineffective in metastatic pMMR tumors, showing a 0% (0/18) response rate to monotherapy with PD-1 blockade[31], and 5% (1/20) response rate to combination treatment with CTLA-4 and PD-1 blockade[32]. The lack of substantial activity in pMMR tumors has previously been correlated to the low TMB and lack of TCI in these tumors[31]. However, the current data indicate that at least a subset of early-stage pMMR CCs with a low TMB and low number of indels is prone to ICI-induced immune recognition, with remarkable pathological down-staging in 4 weeks. In our cohort, $CD8^+PD\text{-}1^+$ TCI was predictive of response in pMMR tumors and, if validated in a larger cohort, may help in selecting patients with pMMR tumors for future neoadjuvant ICI studies.

Furthermore, in nonresponding pMMR tumors, increases in $CD8^+$ T cell counts, TCR clonality, IFN-γ score and CXCL13 expression reflect an underlying immune activation despite little or no tumor regression, in turn suggestive of tumor recognition. Previous work in melanoma has shown that an increase in $CD8^+$ TCI after the start of ICI is associated with a clinical response[8,12]. In particular, step-wise accumulation of $CD8^+$ T cells, starting at the tumor-invasive margin, followed by infiltration to the core of the tumor, was seen in delayed responders, but not in nonresponders. With this perspective, a longer duration of treatment may potentially further increase response rates in pMMR tumors. Possible explanations for nonresponse are a suppressive TME, for example due to COX-mediated immune evasion or high TGF-β expression. The inhibition of COX-2 in our study using celecoxib, albeit in a small number of patients, does not seem to improve responses[16]. Future analyses will focus on dissecting the mechanisms behind immune evasion in nonresponding pMMR tumors to help guide future combinations. Inhibition of TGF-β in combination with ICI might provide a next step in the treatment of pMMR tumors.

The limitations of our study are mainly the small number of patients and the short postoperative follow-up. Larger studies and at least a 3-year follow-up for disease-free survival, a widely accepted surrogate for overall survival in CCs, are required to determine whether the observed MPRs in dMMR and pMMR tumors translate into improved disease-free and overall survival, and whether the changes in the TME of nonresponding pMMR tumors are associated with improved survival.

Future studies in dMMR tumors will focus on establishing efficacy of neoadjuvant immunotherapy compared with the current standard of either adjuvant chemotherapy or surgery only for stage III and II tumors, respectively. The striking lack of response to neoadjuvant chemotherapy in dMMR tumors in the FOXTROT study, and the 100% response rate to neoadjuvant immunotherapy in the present study, should prompt further investigations and larger trials. For pMMR tumors, the NICHE study will be amended to include new combinations of ICI, or ICI with targeted therapies, based on emerging data. The establishment of autologous T cell–tumor organoid cultures from nonresponding patients may help in deciphering causes of resistance, and thus help identify potentially targetable vulnerabilities.

Neoadjuvant immunotherapy in early-stage CCs warrants further research and, when validated in larger studies with longer follow-up, may become a new standard of care in dMMR and possibly a subgroup of pMMR CCs.

Online content

Any methods, additional references, Nature Research reporting summaries, source data, extended data, supplementary information, acknowledgements, peer review information; details of author contributions and competing interests; and statements of data and code availability are available at https://doi.org/10.1038/s41591-020-0805-8.

Received: 27 May 2019; Accepted: 18 February 2020;
Published online: 6 April 2020

References

1. Overman, M. J. et al. Durable clinical benefit with nivolumab plus ipilimumab in DNA mismatch repair-deficient/microsatellite instability-high metastatic colorectal cancer. *J. Clin. Oncol.* **36**, 773–779 (2018).
2. Overman, M. J. et al. Nivolumab in patients with metastatic DNA mismatch repair-deficient or microsatellite instability-high colorectal cancer (CheckMate 142): an open-label, multicentre, phase 2 study. *Lancet Oncol.* **18**, 1182–1191 (2017).
3. Diaz, L. A. Jr. & Le, D. T. PD-1 blockade in tumors with mismatch-repair deficiency. *NEJM* **373**, 1979 (2015).
4. Germano, G. et al. Inactivation of DNA repair triggers neoantigen generation and impairs tumour growth. *Nature* **552**, 116–120 (2017).
5. Mandal, R. et al. Genetic diversity of tumors with mismatch repair deficiency influences anti-PD-1 immunotherapy response. *Science* **364**, 485–491 (2019).
6. Maby, P. et al. Correlation between density of CD8+ T-cell Infiltrate in microsatellite unstable colorectal cancers and frameshift mutations: a rationale for personalized immunotherapy. *Cancer Res.* **75**, 3446–3455 (2015).
7. Fabrizio, D. A. et al. Beyond microsatellite testing: assessment of tumor mutational burden identifies subsets of colorectal cancer who may respond to immune checkpoint inhibition. *J. Gastrointest. Oncol.* **9**, 610–617 (2018).
8. Tumeh, P. C. et al. PD-1 blockade induces responses by inhibiting adaptive immune resistance. *Nature* **515**, 568–571 (2014).
9. Taube, J. M. et al. Association of PD-1, PD-1 ligands, and other features of the tumor immune microenvironment with response to anti-PD-1 therapy. *Clin. Cancer Res.* **20**, 5064–5074 (2014).
10. Blank, C. U. et al. Neoadjuvant versus adjuvant ipilimumab plus nivolumab in macroscopic stage III melanoma. *Nat. Med.* **24**, 1655–1661 (2018).
11. Amaria, R. N. et al. Neoadjuvant immune checkpoint blockade in high-risk resectable melanoma. *Nat. Med.* **24**, 1649–1654 (2018).
12. Huang, A. C. et al. A single dose of neoadjuvant PD-1 blockade predicts clinical outcomes in resectable melanoma. *Nat. Med.* **25**, 454–461 (2019).
13. Powles, T. et al. Clinical efficacy and biomarker analysis of neoadjuvant atezolizumab in operable urothelial carcinoma in the ABACUS trial. *Nat. Med.* **25**, 1706–1714 (2019).
14. Forde, P. M., Chaft, J. E. & Pardoll, D. M. Neoadjuvant PD-1 blockade in resectable lung cancer. *NEJM* **379**, e14 (2018).
15. Mlecnik, B. et al. Integrative analyses of colorectal cancer show immunoscore is a stronger predictor of patient survival than microsatellite instability. *Immunity* **44**, 698–711 (2016).
16. Zelenay, S. et al. Cyclooxygenase-dependent tumor growth through evasion of immunity. *Cell* **162**, 1257–1270 (2015).
17. Cottrell, T. R. et al. Pathologic features of response to neoadjuvant anti-PD-1 in resected non-small-cell lung carcinoma: a proposal for quantitative immune-related pathologic response criteria (irPRC). *Ann. Oncol.* **29**, 1853–1860 (2018).
18. Tetzlaff, M. T. et al. Pathological assessment of resection specimens after neoadjuvant therapy for metastatic melanoma. *Ann. Oncol.* **29**, 1861–1868 (2018).
19. Thommen, D. S. et al. A transcriptionally and functionally distinct $PD\text{-}1^+$ $CD8^+$ T cell pool with predictive potential in non-small-cell lung cancer treated with PD-1 blockade. *Nat. Med.* **24**, 994–1004 (2018).
20. Tauriello, D. V. F. et al. TGFbeta drives immune evasion in genetically reconstituted colon cancer metastasis. *Nature* **554**, 538–543 (2018).
21. Mariathasan, S. et al. TGFbeta attenuates tumour response to PD-L1 blockade by contributing to exclusion of T cells. *Nature* **554**, 544–548 (2018).
22. Mooi, J. K. et al. The prognostic impact of consensus molecular subtypes (CMS) and its predictive effects for bevacizumab benefit in metastatic colorectal cancer: molecular analysis of the AGITG MAX clinical trial. *Ann. Oncol.* **29**, 2240–2246 (2018).
23. Guinney, J. et al. The consensus molecular subtypes of colorectal cancer. *Nat. Med.* **21**, 1350–1356 (2015).

24. Dijkstra, K. K. et al. Generation of tumor-reactive T cells by co-culture of peripheral blood lymphocytes and tumor organoids. *Cell* **174**, 1586–1598 (2018).
25. Jorritsma, A. et al. Selecting highly affine and well-expressed TCRs for gene therapy of melanoma. *Blood* **110**, 3564–3572 (2007).
26. Cloughesy, T. F. et al. Neoadjuvant anti-PD-1 immunotherapy promotes a survival benefit with intratumoral and systemic immune responses in recurrent glioblastoma. *Nat. Med.* **25**, 477–486 (2019).
27. Blank, C. U., Haanen, J. B., Ribas, A. & Schumacher, T. N. Cancer immunology. The 'cancer immunogram'. *Science* **352**, 658–660 (2016).
28. Morton, D. FOxTROT: an international randomised controlled trial in 1052 patients evaluating neoadjuvant chemotherapy for colon cancer. *Ann. Oncol.* **30**(Suppl_5), v198–v252 (2019).
29. Andre, T. et al. Adjuvant fluorouracil, leucovorin, and oxaliplatin in stage II to III colon cancer: updated 10-year survival and outcomes according to BRAF mutation and mismatch repair status of the MOSAIC study. *J. Clin. Oncol.* **33**, 4176–4187 (2015).
30. Sinicrope, F. A. et al. Prognostic impact of deficient DNA mismatch repair in patients with stage III colon cancer from a randomized trial of FOLFOX-based adjuvant chemotherapy. *J. Clin. Oncol.* **31**, 3664–3672 (2013).
31. Le, D. T. et al. PD-1 blockade in tumors with mismatch-repair deficiency. *NEJM* **372**, 2509–2520 (2015).
32. Overman, M. et al. Nivolumab alone or in combination with ipilimumab treatment efficacy, safety, and biomarkers in patients with metastatic colorectal cancer with and without high microsatellite instability: results from the CheckMate 142 study. *Ann. Oncol.* **27**, 149–206 (2016).
33. Ayers, M. et al. IFN-gamma-related mRNA profile predicts clinical response to PD-1 blockade. *J. Clin. Invest.* **127**, 2930–2940 (2017).

Methods

Patient population. Eligible patients were aged 18 years and older and had stage I, II or III resectable colon adenocarcinoma. All patients had an Eastern Cooperative Oncology Group performance-status score of 0 or 1 and adequate end-organ function. Key exclusion criteria were clinical signs of bowel obstruction, immunosuppressive treatment, immunodeficiency, active autoimmune disease and active other cancer.

Study design. This investigator-initiated study was carried out at the Netherlands Cancer Institute (NKI), in collaboration with the Onze Lieve Vrouwe Gasthuis (OLVG). In the run-in part of the study, three patients, regardless of MMR status, were assigned to receive nivolumab monotherapy at a dose of 3 mg kg^{-1} on D1 and D15. All other patients received combination treatment with ipilimumab 1 mg kg^{-1} on D1 + nivolumab 3 mg kg^{-1} on D1 and D15, and patients with pMMR tumors were additionally randomly assigned to receive celecoxib 200 mg daily from D1 until the day before surgery, together with ipilimumab/nivolumab. The predefined maximum time from informed consent to surgery was 6 weeks. For this exploratory, hypothesis-generating study, no formal sample size calculation was performed for efficacy, because there were no data on neoadjuvant immunotherapy and the expected effect size in colon cancer. Based on the expected accrual of patients in a period of 2 years, the present study aimed to include 60 patients total, of whom 30 with pMMR tumors and 30 dMMR tumors (see Extended Data Fig. 1). The NICHE study is currently still enrolling and, based on emerging results, can be adapted to include other treatment combinations and expand cohorts accordingly.

Endpoints and statistics. Primary objectives were safety and feasibility. All patients were closely monitored for AEs until 100 d after the administration of the last nivolumab dose, according to the Common Terminology Criteria for Adverse Events (CTCAE) v.4.03 (ref. [34]). The most severe toxicity grade over all cycles according to the CTCAE criteria v.4.03 was depicted by body system. Safety was assessed by evaluation of AEs and serious AEs, and feasibility was determined based on any treatment-related complications leading to delays in surgery past the 6 weeks after informed consent, or unexpected postsurgery complications. National guidelines indicate that 'a treatment' should be started within 5 weeks of diagnosis of a CC. In our institute the median time to any treatment was an average of 6 weeks for patients not treated within this study. Safety and feasibility were evaluated after the first three patients in the run-in period had undergone surgery and were released from hospital, and the local ethics board approved further accrual. This procedure was repeated after a total of six patients had been included. After establishing safety and feasibility in the first six patients according to the primary endpoint, accrual was continued into an exploratory expansion cohort.

Secondary and translational endpoints included efficacy, as assessed by histopathological response to treatment, and associations between response and immunological, morphological and genomic findings, including TMB, IFN-γ gene signatures, TCI and TCR clonality.

All patients underwent baseline tumor staging, consisting of CT imaging of the chest and abdomen. Pretreatment tumor biopsies were taken during colonoscopies. Posttreatment tissue was obtained at surgery. Samples were immediately frozen or formalin fixed and paraffin embedded. The whole tumor bed was submitted for histopathological analysis. When indicated by positive lymph node or T4 status posttreatment, patients were offered adjuvant chemotherapy. All patients were followed for recurrence and survival.

Differences between pMMR and dMMR tumors were analyzed using the (nonparametric) Wilcoxon's rank-sum test (Mann–Whitney *U*-test), whereas differences between post- and premeasurements within a group were analyzed using Wilcoxon's signed-rank test. For comparisons across multiple groups a Kruskal–Wallis test was performed.

Comparison of categorical variables was performed using Fisher's two-sided exact test. For binary outcomes, 95% two-sided CIs were constructed using the Clopper–Pearson method. Median follow-up from time of enrollment was calculated using the reverse Kaplan–Meier method. Analyses were performed using R v.3.5.1. All reported *P* values are two sided and, in all cases, a *P* value <0.05 was required for statistical significance. For comparisons of TMB and number of indels, medians and IQRs are provided. No adjustments were made for multiple comparisons.

Study oversight. The study protocol was approved by the local ethics board of the NKI (sponsor) and was conducted in accordance with the ICH Harmonised Tripartite Guideline for Good Clinical Practice and the principles of the Declaration of Helsinki. All patients provided written informed consent.

Pathology assessments and IHC analyses. Formalin-fixed, paraffin-embedded (FFPE) sections were obtained from both pretreatment biopsies and resection specimens. Baseline tumor biopsies were used to assess MMR status using IHC for MLH1, PMS2, MSH2 and MSH6 according to standard protocols for the Ventana automated immunostainer (MLH1 Ready-to-Use, M1, 6472966001, lot no. G07286, Roche; MSH2, Ready-to-Use, G219-1129, 5269270001, lot no. 1616008C, Roche; MSH6, 1/50 dilution, EP49, AC-0047, lot no. EN020910, Abcam; PMS2, 1/40 dilution, EP51, M3647, lot no. 1012289, Agilent Technologies).

Primary colon tumors and lymph nodes were staged according to the American Joint Committee on Cancer (8th edition)[35]. Histopathological examination of biopsies and resection specimens was carried out by two experienced gastrointestinal pathologists. Slides were counterstained with Hematoxylin and Bluing Reagent (Ventana Medical Systems). Resected tumors were examined in their entirety and regression of resected tumors was assessed by estimating the percentage of residual viable tumor of the macroscopically identifiable tumor bed, as identified on routine hematoxylin and eosin (H&E) staining[17]. In addition, regression was classified using the Mandard tumor regression grading system[36]. MPR was defined as ≤10% of residual viable tumor, corresponding to Mandard tumor regression grade 1 (CR) or 2 (near-CR). PR was defined as at least 50% tumor regression. However, considering the lack of consensus on the definition of PR after immunotherapy, with cut-offs for PR at either ≥50% tumor regression in melanoma[18] or ≥10% tumor regression in lung cancer[17], tumors with >50% and <90% residual viable tumor were labeled accordingly as '10–50% tumor regression'. When analyzing pMMR responders versus pMMR nonresponders, this subgroup is included in the group of nonresponders.

FFPE specimens were additionally examined by IHC analysis of CD3, CD8, FOXP3, PD-1, PD-L1, CD68 and CD20 using consecutively sectioned slides to enable comparison of infiltrates. In brief, FFPE sections were cut at 3 µm, heated at 75 °C for 28 min and deparaffinized in the instrument with EZ prep solution (Ventana Medical Systems). Heat-induced antigen retrieval was carried out using Cell Conditioning 1 (CC1, Ventana Medical Systems) for 32 min at 95 °C (CD3, CD8, CD68, CD20), 48 min at 95 °C (PD-1 and PD-L1) or 64 min at 95 °C (FOXP3). CD3 was detected using clone SP7 (Spring/ITK, 1/100 dilution, 32 min at 37 °C, lot no. 160407LVP), CD8 by using clone C8/144B (DAKO/Agilent, 1/200 dilution, 32 min at 37 °C, lot no. 20066516), CD68 using clone KP1 (DAKO/Agilent, 1/10,000 dilution, 32 min at 37 °C, lot no. 20040389), FOXP3 using clone 236A/E7 (Abcam, 1/200 dilution 2 h at room temperature, lot no. GR3220121-1), PD-1 using clone NAT105 (Cell Marque/Roche, Ready-to-Use, 16 min at room temperature, lot no. V0001234), PD-L1 using clone 22C3 (DAKO/Agilent, 1/40 dilution, 1 h at room temperature, lot no. 10137461) and CD20 using clone L26 (DAKO/Agilent, 1/800 dilution, 32 min at 37 °C, lot no. 20038880), all followed by 3,3′-diaminobenzidine (DAB) detection.

For the assessment of T cell infiltrates and digital quantitation of each T cell subtype, FFPE slides with at least two tumor biopsies per slide were chosen for IHC staining, and immunostained slides were scanned at high resolution on a CD-IVD-certified Philips Ultra-Fast Scanner 300 (Philips Digital Pathology Solutions) and digital image analysis was performed using the HALO image analysis software, v.2.0.1145.19 (Indica Labs). CD3-, CD8- and FOXP3-stained serial tissue sections were co-registered (in HALO) and manual annotations of the identified tumor areas were automatically transferred to aligned sections, annotating the entire tumor area in the respective slides, excluding the invasive margin. Areas were carefully selected not to contain folds. DAB-positive cells were quantified using the HALO multiplex algorithm v.1.2. Results presented in the present study were obtained by measuring entire tumor areas in the resection slides.

For the double-staining of PD-1 (yellow) followed by CD8 (purple), the PD-1 was detected in the first sequence using clone NAT105 (Ready-to-Use, 32 min at 37 °C, Roche Diagnostics). PD-1-bound antibody was visualized using anti-mouse NP (Ventana Medical systems) for 12 min at 37 °C followed by anti-NP AP (Ventana Medical systems) for 12 min at 37 °C, followed by the Discovery Yellow Detection Kit (Ventana Medical Systems). In the second sequence of the double-staining procedure, CD8 was detected using clone C8/144B (Agilent, 1:200 dilution, 32 min at 37 °C). CD8 was visualized using anti-mouse HQ (Ventana Medical systems) for 12 min at 37 °C followed by anti-HQ horseradish peroxidase (Ventana Medical systems) for 12 min at 37 °C, followed by the Discovery Purple Detection Kit (Ventana Medical Systems). Slides were counterstained with Hematoxylin and Bluing Reagent (Ventana Medical Systems). Additional information on antibodies used is provided in the Nature Research Reporting Summary.

The presence of TLSs, defined as CD20$^+$ lymphoid aggregates (≥100 lymphocytes) with a germinal center, was assessed on CD20-stained slides sections for both pretreatment biopsies and posttreatment resection specimens. The presence of TLSs[17] was quantitatively scored.

Genetic and transcriptional profiling. Whole-exome sequencing was performed on pretreatment tumor DNA samples and matched peripheral blood samples. RNA from pre- and posttreatment samples was used to assess TCI, CMSs, IFN-γ-related immune-gene signatures and TGF-β signatures, and for single-gene analyses.

DNA and RNA were extracted from fresh-frozen, pre- and posttreatment tumor material using the AllPrep DNA/RNA Kit (QIAGEN) for frozen material, following the manufacturer's protocol, in a QIAcube (QIAGEN). Germline DNA was isolated from patient PBMCs using the DNeasy Blood & Tissue Kit (QIAGEN). Fresh-frozen samples for DNA and RNA extraction were chosen based on a tumor percentage of at least 30%, except for posttreatment samples of tumors with a complete response. DNA was fragmented to 200- to 300-base pair (bp) fragments by Covaris DNA shearing, after which library preparation was performed using KAPA HTP/LTP DNA Library Kit (Roche), according to the manufacturer's instructions.

Exome enrichment was performed using the xGen Exome Research Panel kit (IDT) according to the manufacturer's instructions. Libraries were sequenced with 100-bp paired-end reads on a HiSeq 2500 in high output mode using V2 chemistry, with a median sequencing depth of 90-fold (range: 51, 105). Raw reads were aligned to GRCh38 using the Burrows–Wheeler aligner[37], followed by marking of duplicate reads by Picard MarkDuplicates (http://broadinstitute.github.io/picard). Subsequently, base quality scores were recalibrated using BaseRecalibrator and variants were called using MuTect2 (ref. [38]). Nonsynonymous TMB was determined by summing the coding, nonsynonymous, single-nucleotide variants and frame-shifting indels, and is shown as the absolute number of mutations.

Strand-specific libraries were generated using the TruSeq Stranded mRNA Sample Prep Kit (Illumina) according to the manufacturer's instructions. Poly(adenylated) RNA from intact total RNA was purified using oligo(dT) beads. After purification, the RNA was fragmented, random primed and reverse transcribed using SuperScript II Reverse Transcriptase (Thermo Fisher Scientific) with the addition of dactinomycin. Second-strand synthesis was performed using polymerase I and RNaseH, replacing deoxythymidine triphosphate with deoxyuridine triphosphate. The generated complementary DNA fragments were 3′-end adenylated and ligated to Illumina paired-end sequencing adapters, and subsequently amplified by 12 cycles of PCR. Libraries were analyzed on a 2100 Bioanalyzer using a 7,500 chip (Agilent), diluted, pooled equimolar into a multiplex sequencing pool and stored at −20 °C. Libraries were sequenced with 65-bp, single-end reads on a HiSeq 2500 System in high output mode using V4 chemistry (Illumina). Raw reads were aligned to GRCh38 using STAR RNA-sequencing aligner, after which gene expression levels were quantified using default parameters for both applications.

The 'Expanded Immune' signature from Ayers et al.[33] was used to perform hierarchical clustering on normalized gene expression values. Gene-level expression values were computed as transcripts per million (TPM) and normalized to *Z*-scores before clustering. Associated IFN-γ scores were calculated by summation of the *Z*-scores of all signature genes for each individual sample. TGF-β signatures[39] were computed by averaging *Z*-scores for each individual gene in the signature.

CMS subtyping was performed using a 58,233 × 40 gene expression matrix in TPM units summarized per gene. Genes that were not expressed in all samples were removed, after which sequencing depth was normalized using the median-of-ratios method, as implemented in the DESeq2 R package[40] (R package v.1.22.2). Ensembl ids were converted to the HUGO Gene Nomenclature Committee gene symbols using the biomaRt R package (v.biomaRt_2.38.0) and Ensembl v.95 (current as of January 2019). To assign CMSs to each sample the random Forest method from the Sage Bionetworks CMSclassifier (v.1.0.0) was used. Reported are posterior probabilities per subtype, nearest subtype and predicted subtype per sample[23,40,41].

TCR sequencing. TCR sequencing was performed on pre- and posttreatment samples to assess clonality and changes herein in correlation with response. Immunosequencing of the CDR3 regions of human TCR-β chains was performed on pre- and posttreatment biopsies using the ImmunoSEQ Assay (Adaptive Biotechnologies). For 13 patients (14 tumors due to patient with double tumor), TCR sequencing was performed on PBMCs pre- and posttreatment in addition to pre- and posttreatment tissue. Extracted genomic DNA was amplified in a bias-controlled multiplex PCR, followed by high-throughput sequencing. Nucleotide sequences were collapsed and filtered to identify and quantify the abundance of each unique TCR-β CDR3 region for further analysis. The frequency of productive rearrangements was summed with identical CDR3 amino acid sequences, and the resulting frequencies were normalized to the total nucleated cell estimate.

Organoid establishment. Tumor organoids were established from pretreatment biopsies (NICHE-2, -7, -3_dMMR, -10, -11, -12, -26, -35 and -39) or posttreatment surgical resection specimens (NICHE-3_pMMR, -11 and -38)[24]. Briefly, tumor tissue was mechanically dissociated and digested with 1.5 mg ml^{-1} of collagenase II (Sigma-Aldrich), 10 μg ml^{-1} of hyaluronidase type IV (Sigma-Aldrich) and 10 μM Y-27632 (Sigma-Aldrich). Cells were embedded in Geltrex (Geltrex LDEV-free reduced growth factor basement membrane extract, Gibco) and placed in a 37 °C incubator for 20 min. Cells were then overlaid with human CRC organoid medium[42], composed of Advanced Dulbecco's modified Eagle's medium/F12 (Gibco), 2 mM Ultraglutamine I (Lonza), 10 mM 4-(2-hydroxyethyl)-1-piperazine-ethanesulfonic acid (Gibco), 100/100 U ml^{-1} of penicillin–streptomycin (Gibco), 10% Noggin-conditioned medium, 20% R-spondin1-conditioned medium, 1× B27 supplement without vitamin A (Gibco), 1.25 mM *N*-acetylcysteine (Sigma-Aldrich), 10 mM nicotinamide (Sigma-Aldrich), 50 ng ml^{-1} of human recombinant epidermal growth factor (Peprotech), 500 nM A83-01 (Tocris), 3 μM SB202190 (Cayman Chemicals), 10 nM PGE_2 (Cayman Chemicals) and 1:500 Primocin (Invivogen). Organoids were passaged every 1–2 weeks by incubating in TrypLE Express (Gibco) for 5–10 min followed by embedding in Geltrex. Organoids were authenticated by SNP array as described in Dijkstra et al.[24] and regularly tested for *Mycoplasma* spp. using *Mycoplasma* PCR[43] and the MycoAlert Mycoplasma Detection Kit (catalog no. LT07-318). A positive result in one of the two tests was sufficient to reject the sample. Organoids that could not be authenticated or were *Mycoplasma* contaminated were excluded from analysis (see Supplementary Table 5).

Patient-derived T cells. PBLs were isolated from peripheral blood using Ficoll–Paque and cryopreserved for later use. Blood was drawn before treatment and at the time of surgery. For NICHE-3, blood was obtained after the first cycle of nivolumab. For NICHE-3, TILs were expanded as described previously[44], using 1 week of T cell expansion in high-dose (6,000 U ml^{-1}) interleukin (IL)-2, followed by 2 weeks of expansion after stimulation with irradiated feeder cells (healthy donor PBMCs) and 30 ng ml^{-1} of OKT-3, in the presence of 3,000 U ml^{-1} of IL-2. NICHE-3 is the same patient as CRC-13 in a previous publication from our group where tumor reactivity of pretreatment blood was reported[24].

MART-1-specific T cells. For the production of MART-1-specific (1D3) T cells, MART-1 TCR retrovirus was harvested from the supernatant of a producer cell line[45]. PBMCs were isolated from the blood of healthy donors (Sanquin) by Ficoll–Paque density gradient centrifugation. PBLs enriched for $CD8^+$ T cells (Dynabeads $CD8^+$ isolation kit) were cultured in T cell medium supplemented with 500 U ml^{-1} of IL-2, in a nontissue culture-treated, 24-well plate coated with 5 μg ml^{-1} of anti-CD3 and 5 μg ml^{-1} of anti-CD28. After 48 h, T cells (1.5×10^6 ml^{-1}) were mixed 1:1 with retrovirus, plated on a retronectin-coated (Takara, 25 μg per well), nontissue culture-treated, 24-well plate, and spun for 90 min at 600*g*. After 24 h, T cells were washed and expanded for 2 weeks at 1.5×10^6 ml^{-1} in T cell medium supplemented with 500 U ml^{-1} of IL-2.

Organoid–lymphocyte co-culture. PBLs and tumor organoids were co-cultured as previously described[24]. Tumor organoids were isolated from Geltrex by incubating in 2 mg ml^{-1} of type II dispase (Sigma-Aldrich) for 15 min 2 d before addition of the PBLs. After incubation, 5 mM ethylenediaminetetraacetic acid (EDTA) was added, and organoids were washed and plated in CRC or normal colon organoid medium in the presence of 10 μN Y-27632. A day before co-culture, organoids were stimulated with 200 ng ml^{-1} of IFN-γ (Peprotech). Organoids were dissociated into single cells and plated at a 1:20 target:effector ratio with autologous PBLs, in an anti-CD28-coated (clone CD28.2, eBioscience), 96-well, U-bottomed plate, in the presence of 150 U ml^{-1} of IL-2 (Proleukin) and 20 μg ml^{-1} of anti-PD-1 (Merus). Half of the medium was refreshed every 2–3 d with addition of new IL-2 and anti-PD-1, and PBLs were collected and re-stimulated as above after 1 week of co-culture.

Tumor recognition assay. After 2 weeks of co-culture, tumor organoids were prepared and dissociated into single cells as above. T cells were collected and stimulated with tumor or healthy colon cells at a 1:2 target:effector ratio in an anti-CD28-coated, 96-well, U-bottomed plate in the presence of 20 μg ml^{-1} of anti-PD-1 (Merus) and 1:100 mouse anti-human CD107a-PE antibodies (BD Biosciences). After 1 h of incubation, GolgiSTOP (BD Biosciences, 1:1,500) and GolgiPlug (BD Biosciences, 1:1,000) were added. After 4 h of incubation, T cells were washed twice in cold FACS buffer (1% bovine serum antigen + 5 mM EDTA in phosphate-buffered saline (PBS)) and stained with 1:20 anti-CD3-PerCP-Cy5.5 (BD Biosciences), 1:20 anti-CD4-FITC (BD), 1:200 anti-CD8-BV421 (BD Biosciences) and 1:2,000 near-infrared viability dye (Life Technologies) for 30 min at 4 °C. Cells were washed, fixed and stained with 1:40 anti-IFN-γ-APC (BD Biosciences) for 30 min at 4 °C, using the Cytofix/Cytoperm Kit (BD Biosciences). T cells stimulated with 50 ng ml^{-1} of phorbol 12-myristate 13-acetate (Sigma-Aldrich) and 1 μg ml^{-1} of ionomycin (Sigma-Aldrich) served as positive controls.

HLA-A2 transduction. Organoids were lentivirally transduced with HLA-A2 on a lentiviral backbone. The vector also contained β_2-microglobulin with a mutation that renders HLA-A2 insensitive to blocking by W6/32 MHC-I-blocking antibodies. Organoids were dissociated to single cells and resuspended at 5×10^5 ml^{-1} in Ad-DF^{+++}. Cells were combined with 24 μl of 40× concentrated HLA-A2 virus per 1×10^6 cells, in the presence of 8 μg ml^{-1} of protamine sulfate (Sigma-Aldrich) and 10 μM Y-27632. After mixing by resuspension, 500 μl of cell suspension was plated per well of a 48-well plate, centrifuged for 1 h at room temperature (100*g*), and plated overnight. The next day, cells were collected (using TrypLE to detach cells that have attached to the culture plate), centrifuged (400*g*, 5 min, room temperature) and infection medium was discarded. Organoids were plated in Geltrex and cultured as described above.

MART-1 assays. One day before the assay, 1D3 T cells were thawed and maintained overnight in T cell medium supplemented with 150 U ml^{-1} of IL-2 (ref. [46]). Organoids were stimulated with 200 ng ml^{-1} of IFN-γ. The next day, tumor organoids were dissociated to single cells and resuspended at 4×10^5 ml^{-1} in RPMI without serum (Gibco). Anchor-residue-modified MART-1 peptide (ELAGIGILTV)[47] was resuspended at a concentration of 0.2 μg ml^{-1} in RPMI, and an equal volume was added to organoids. After a 30-min incubation at 37 °C, organoids were washed twice in RPMI (500*g*, 5-min centrifugation) and counted again. Organoids were resuspended at 7.5×10^4 ml^{-1} in T cell medium. The 1D3 T cells were counted, washed and resuspended at 1.5×10^6 cells ml^{-1} in T cell medium. Then, 100 μl of MART-1-loaded organoids and 100 μl of 1D3 T cells

were plated in a 96-well, U-bottomed plate and cultured for 24 h (effector:target ratio = 20:1 (7.5×10^3 tumor cells + 1.5×10^6 T cells)).

After 24 h, 10 µl supernatant was collected and IFN-γ concentrations were determined using a human IFN-γ Cytometric Bead Array (CBA, BD Biosciences) following the manufacturer's instructions with a few adaptations. Then 10 µl of supernatant, beads and detection antibody was used, and the assay was performed in 0.5 mM EDTA/PBS. CBA median fluorescence intensities were converted to IFN-γ concentrations based on a standard curve. Data from multiple independent experiments were pooled. Individual dots indicate independent experiments and error bars indicate s.e.m.

Flow cytometry and cell sorting. T cells assayed for tumor reactivity, beads used in CBA or organoids stained for HLA-ABC or HLA-A2 were recorded on a Becton Dickinson Fortessa flow cytometer. For evaluation of HLA expression, organoids were dissociated to single cells using TrypLE Express, washed twice in ice-cold FACS buffer and stained with 1:20 mouse anti-human HLA-A, -B or -C-PE (BD Biosciences), 1:20 mouse anti-human HLA-A2-APC (BD Biosciences) or 1:20 isotype controls (PE or APC mouse IgG1, kappa (BD Biosciences)). Tumor cells were incubated for 30 min at 4 °C in the dark and washed twice in FACS buffer. Before flow cytometric recording, 1:50 DAPI was added.

In some experiments, tumor cells were stained with 1:2,000 near-infrared viability dye at the same time as staining for HLA molecules. Cells were then washed and fixed for 20 min at 4 °C using the Cytofix/Cytoperm Kit (BD Biosciences). Cells were washed twice in FACS buffer and recorded on a flow cytometer after a maximum of 24 h. HLA-A2-transduced organoids were sorted to similar HLA-A2 expression levels using FACSAria Fusion.

Reporting Summary. Further information on research design is available in the Nature Research Reporting Summary linked to this article.

Data availability

The RNA- and DNA-sequencing data will be deposited into the European Genome–Phenome Archive under accession no. EGAS00001004160 and will be made available on reasonable request for academic use and within the limitations of the provided informed consent. Every request will be reviewed by the institutional review board of the NKI; the researcher will need to sign a data access agreement with the NKI after approval. The TCR-sequencing data that support the findings of the present study are available from Adaptive Biotechnologies; however, restrictions apply to the availability of these data, which were used under license for the present study and are not publicly available. However, data are available from the authors on reasonable request and with the permission of Adaptive Biotechnologies.

References

34. *Revised Common Terminology Criteria for Adverse Events (CTCAE)* Version 4.0 (National Cancer Institute); https://ctep.cancer.gov/protocoldevelopment/electronic_applications/ctc.htm#ctc_40 (2009).
35. Brierley, J., Gospodarowicz, M. K. & Wittekind, C. TNM Classification of Malignant Tumours (John Wiley & Sons, 2017).
36. Mandard, A. M. et al. Pathologic assessment of tumor regression after preoperative chemoradiotherapy of esophageal carcinoma: clinicopathologic correlations. *Cancer* **73**, 2680–2686 (1994).
37. Li, H. & Durbin, R. Fast and accurate short read alignment with Burrows–Wheeler transform. *Bioinformatics* **25**, 1754–1760 (2009).
38. McKenna, A. et al. The genome analysis toolkit: a MapReduce framework for analyzing next-generation DNA sequencing data. *Genome Res.* **20**, 1297–1303 (2010).
39. Calon, A. et al. Dependency of colorectal cancer on a TGF-beta-driven program in stromal cells for metastasis initiation. *Cancer Cell* **22**, 571–584 (2012).
40. Love, M. I., Huber, W. & Anders, S. Moderated estimation of fold change and dispersion for RNA-seq data with DESeq2. *Genome Biol.* **15**, 550 (2014).
41. Guinney, J. et al. The consensus molecular subtypes of colorectal cancer. *Nat. Med.* **21**, 1350–1356 (2015).
42. van de Wetering, M. et al. Prospective derivation of a living organoid biobank of colorectal cancer patients. *Cell* **161**, 933–945 (2015).
43. Young, L., Sung, J., Stacey, G. & Masters, J. R. Detection of Mycoplasma in cell cultures. *Nat. Protoc.* **5**, 929–934 (2010).
44. Dudley, M. E., Wunderlich, J. R., Shelton, T. E., Even, J. & Rosenberg, S. A. Generation of tumor-infiltrating lymphocyte cultures for use in adoptive transfer therapy for melanoma patients. *J. Immunother.* **26**, 332–342 (2003).
45. Gomez-Eerland, R. et al. Manufacture of gene-modified human T-cells with a memory stem/central memory phenotype. *Hum. Gene Ther. Methods* **25**, 277–287 (2014).
46. Cattaneo, C. M. et al. Tumor organoid-T-cell coculture systems. *Nat. Protoc.* **15**, 15–39 (2020).
47. Romero, P. et al. Antigenicity and immunogenicity of Melan-A/MART-1 derived peptides as targets for tumor reactive CTL in human melanoma. *Immunol. Rev.* **188**, 81–96 (2002).

Acknowledgements

We thank all patients and their families for participating in the present study. We thank: the Core Facility of Molecular Pathology and Biobanking, L. Braaf, S. Cornelissen and D. Peters for their support in processing of samples; C. Van Rooijen for setting up CD8/PD-1 co-stains; R. Kerkhoven and the Genomics Core Facility for their support with sequencing; the Flow Cytometry Core Facility for their support in flow cytometry; J. Lips from Adaptive Biotechnologies for his support; L. Al-van Wijck from the scientific administration department for data management; L. Hoes, F. Weeber, J. Westra, S. Visser and S. Kaing for facilitating sample acquisition and processing; A. Van der Leun for support in TIL isolation; T. Korse, M. Lucas and E. Platte for PBMC acquisition and processing; A. Atsma, P. Bottenberg, S. Oosterloo, M. van Wijngaarden, P. Den Hartog and S. Dokter for patient care; M. Mok, I. Honing, M. Van Nes and N. De Jong for patient care in the OLVG; P. Drillenburg for sample acquisition; Merus for provision of anti-PD-1 for in vitro experiments; M. Toebes, X. Kong and M. Ligtenberg for the lentiviral HLA-A2 vector and MART-1 peptide; S. Vanhoutvin for legal support; A. Evans, D. Tauriello, G. Sonke and H. Van Tinteren for scientific input. The present study was funded by the BMS International Immuno-Oncology Network and sponsored by the NKI. The funding source had no role in design and execution of the study, data analysis or writing of the manuscript.

Author contributions

M.C. designed the trial, coordinated trial procedures, analyzed and interpreted clinical and translational data and wrote the manuscript. L.F.F. performed and interpreted bioinformatics analyses. K.K.D. and V.V. performed organoid experiments. J.G.V.d.B. and P.S. performed the histo- and immunopathological scoring. A.G.A., G.L.B., N.F.K. and H.A.M. informed patients and performed surgery. M.L.-Y. and K.S. performed statistical analyses. C.G. and M. Kuiper were responsible for patient care. M. Maas and R.G.B.-T. revised CT scans. M. Mertz set up digital quantification of IHC staining. G.B. performed CMS subtyping. A.B. provided input on IHC staining. E.N. was the clinical projects manager. W.H.V., T.R.d.W. and M.E.V.L. performed endoscopies. A.U.v.L. informed and referred patients. M. Kok provided scientific input during protocol writing and design of the study. M.C., T.N.S., E.E.V. and J.B.H. made the experimental plan of investigation. The manuscript was written by M.C. in collaboration with co-authors, who vouch for the accuracy of the data reported and adherence to the protocol. All authors edited and approved the manuscript.

Competing interests

L.F.F., K.K.D., J.G.V.d.B., A.G.A., M.L.-Y., K.S., C.G., G.L.B., P.S., M. Mertz, V.V., G.B., A.B., R.G.B.-T., T.R.d.W., A.U.v.L., H.A.M., M. Maas, E.N., N.F.K., W.H.V., A.U.v.L., M. Kuiper and M.E.V.L. have no competing interests to declare. M.C. reports funding to the institute from BMS and Roche/Genentech and an advisory role for BMS, outside the submitted work. M. Kok reports funding to the institute from BMS, Roche/Genentech, AZ and an advisory role for BMS and Daiichi Sankyo, outside the submitted work. J.B.H. reports institutional fees for advisory roles from BMS, Merck, Roche, Neon therapeutics, Pfizer and Ipsen and NKI, and received grants from BMS, Merck, Novartis and Neon Therapeutics, outside the submitted work. E.E.V. reports research funding from BMS, outside the submitted work. T.N.S. is a consultant for Adaptive Biotechnologies, AIMM Therapeutics, Allogene Therapeutics, Amgen, Merus, Neon Therapeutics, Scenic Biotech; Grant/Research support are from: Merck, Bristol-Myers-Squibb, Merck KGaA; stockholder in: AIMM Therapeutics, Allogene Therapeutics, Neon Therapeutics, all outside the submitted work.

Additional information

Extended data is available for this paper at https://doi.org/10.1038/s41591-020-0805-8.

Supplementary information is available for this paper at https://doi.org/10.1038/s41591-020-0805-8.

Correspondence and requests for materials should be addressed to M.C. or E.E.V.

Peer review information Javier Carmona was the primary editor on this article, and managed its editorial process and peer review in collaboration with the rest of the editorial team.

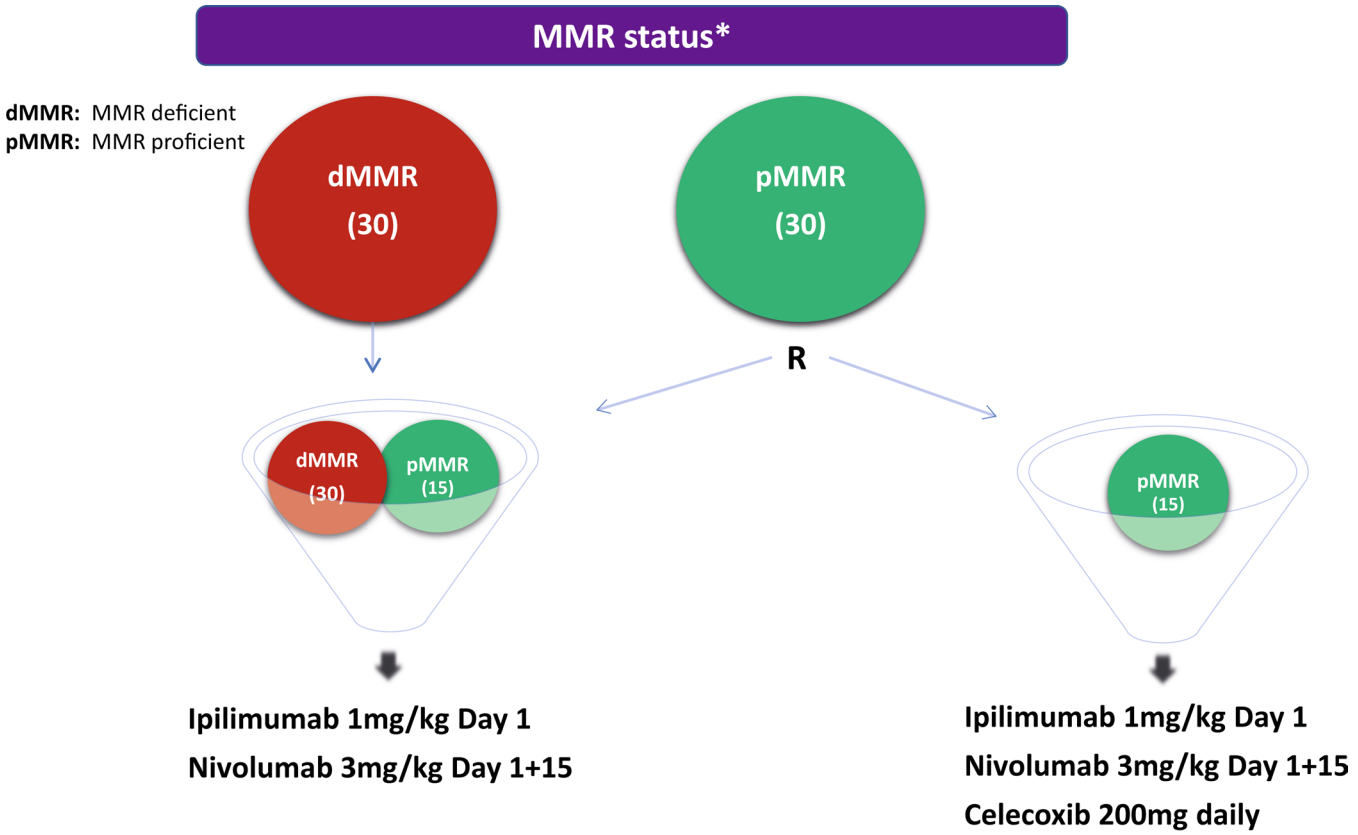

MMR protein staining for MLH1, PMS2, MSH2, MSH6

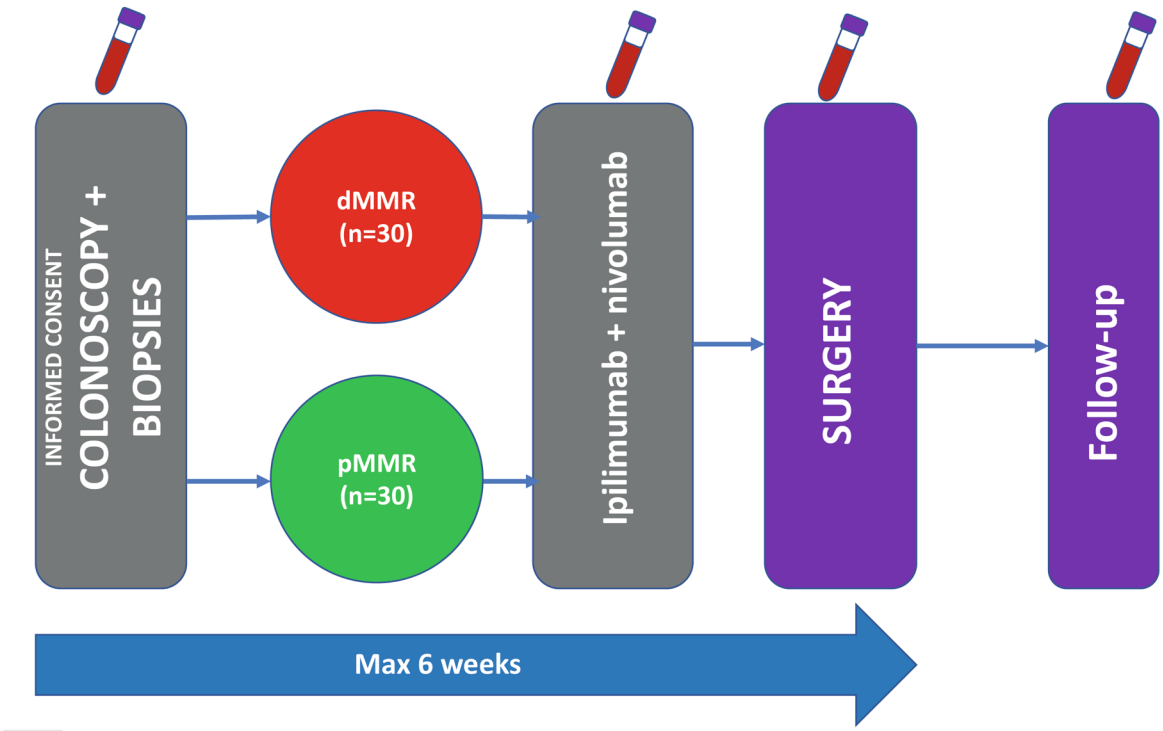

Extended Data Fig. 1 | Study design. Patients with dMMR or pMMR colon cancers were screened after signing informed consent. Maximum duration from informed consent to surgery was 6 weeks. All patients underwent an endoscopy to obtain biopsies. Shortly thereafter, treatment was started (and patients with pMMR tumors randomized to celecoxib yes/no). Numbers shown refer to the total number of patients to be included per subgroup in this ongoing study.

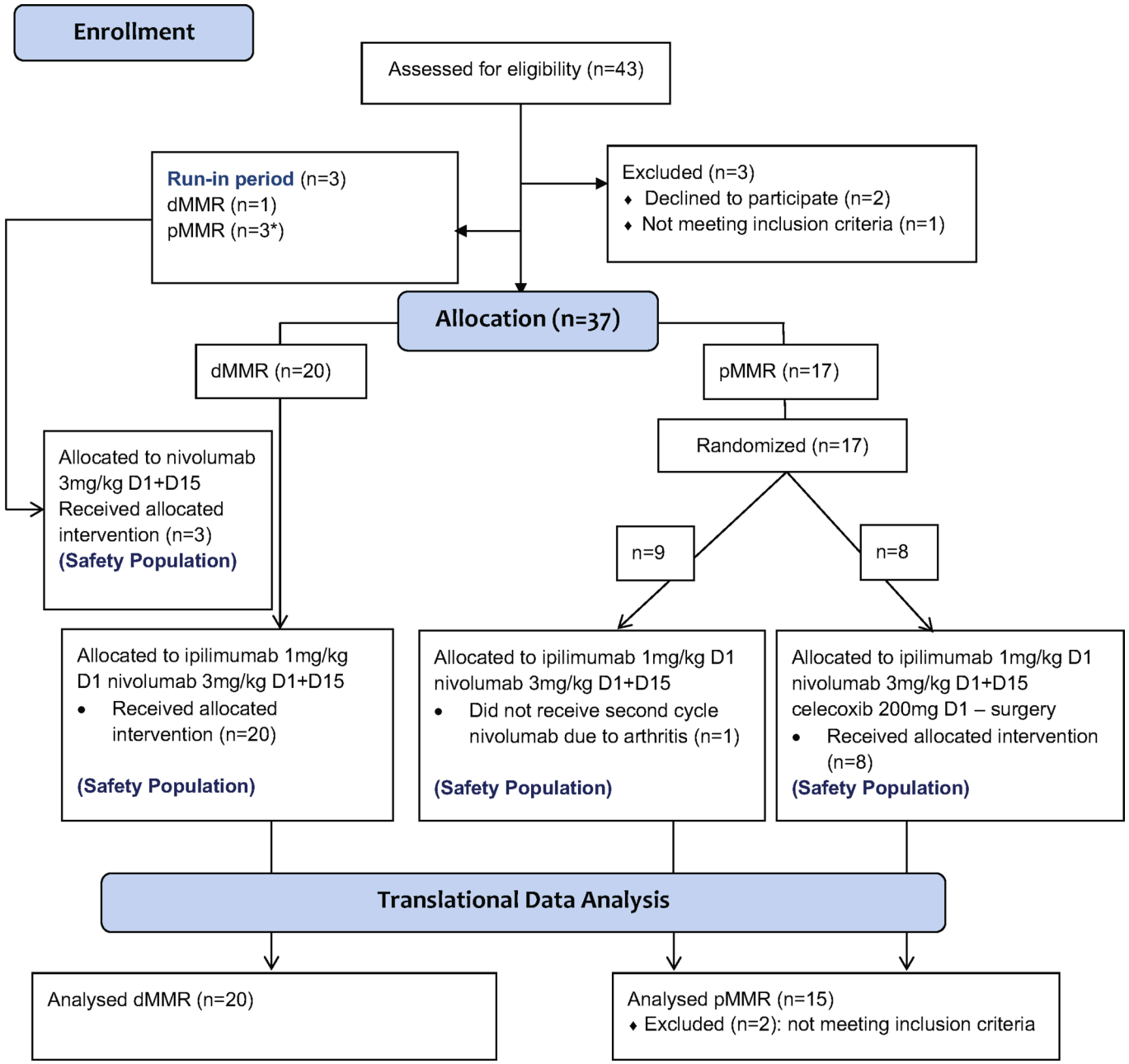

Extended Data Fig. 2 | Consort Diagram. Patient numbers refer to included patients at the time of data cut-off. *Patient in the run-in period with 2 tumors is accounted for as 1 patient in the eligibility assessment in the dMMR group.

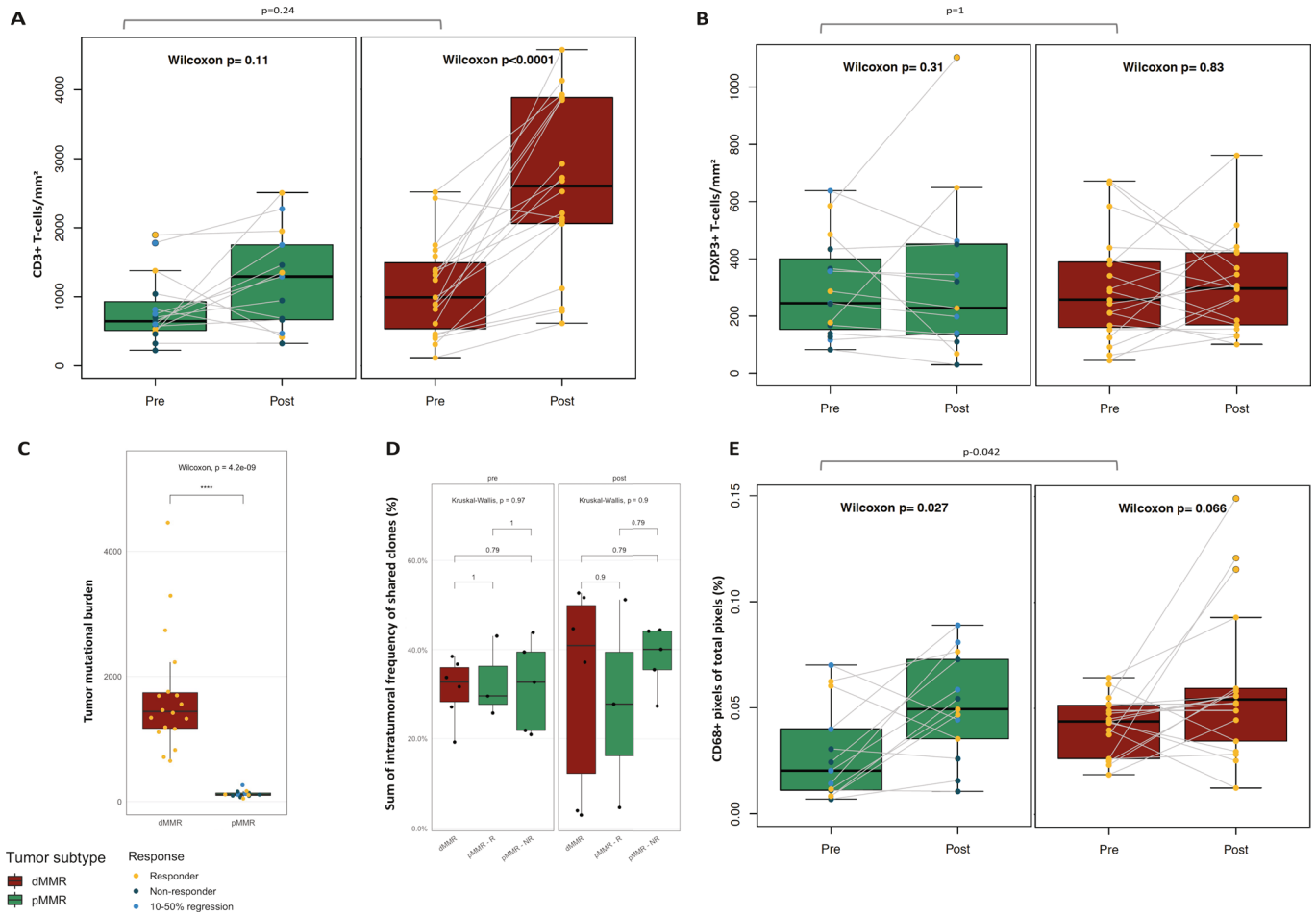

Extended Data Fig. 3 | Characteristics of T-cell infiltration in pMMR and dMMR tumors. Panel **a**, Changes in CD3+ T cell infiltration in pMMR tumors (left, n=13) and dMMR tumors (right, n=19). Boxplots represent the median, 25th and 75th percentiles; the whiskers extend from the hinge to the largest value no further than 1.5 * IQR from the hinge. Pre-to-post pairwise statistical significance was tested with a Wilcoxon Signed-Rank test; for differences between pMMR and dMMR significance was tested using a Wilcoxon Rank-Sum test. All statistical tests were two-sided. Panel **b**, Changes in FOXP3 T cell infiltration in pMMR tumors (left, n=13) and dMMR tumors (right, n=19). Boxplots represent the median, 25th and 75th percentiles; the whiskers extend from the hinge to the largest value no further than 1.5 * IQR from the hinge. Pre-to-post pairwise statistical significance was tested with a Wilcoxon Signed-Rank test; for differences between pMMR and dMMR significance was tested using a Wilcoxon Rank-Sum test. All statistical tests were two-sided. Panel **c**, Tumor mutational burden (absolute number of mutations by summation of coding non-synonymous single nucleotide variants and frame-shifting indels) in dMMR (left, n=19) vs. pMMR (right, n=15) tumors. Boxplots represent the median, 25th and 75th percentiles; the whiskers extend from the hinge to the largest value no further than 1.5 * IQR from the hinge. For differences between dMMR and pMMR, statistical significance was tested with a Wilcoxon Rank-Sum test. All statistical tests were two-sided. Panel **d**, Sum of intratumoral frequency of T cell clones shared between tissue and peripheral blood. Left: pre-treatment and Right: post-treatment comparisons between dMMR (n=6), pMMR responders (pMMR-R, n=3) and pMMR non-responders (pMMR-NR, n=5). Boxplots represent the median, 25th and 75th percentiles; the whiskers extend from the hinge to the largest value no further than 1.5 * IQR from the hinge. Pairwise statistical significance was tested with a Wilcoxon Rank-Sum test, while for comparisons between multiple groups a Kruskal-Wallis test was used. All Wilcoxon statistical tests were two-sided. Panel **e**, CD68 positivity shown in pixel counts as a percentage of total pixel count. Left: pre-to-post treatment changes in pMMR (n=13) and Right: dMMR (n=19) tumors. Boxplots represent the median, 25th and 75th percentiles; the whiskers extend from the hinge to the largest value no further than 1.5 * IQR from the hinge. Pre-to-post pairwise statistical significance was tested with a Wilcoxon Signed-Rank test; for differences between pMMR and dMMR significance was tested using a Wilcoxon Rank-Sum test. All statistical tests were two-sided. Panel **a**-**e**: No adjustments were made for multiple comparisons.

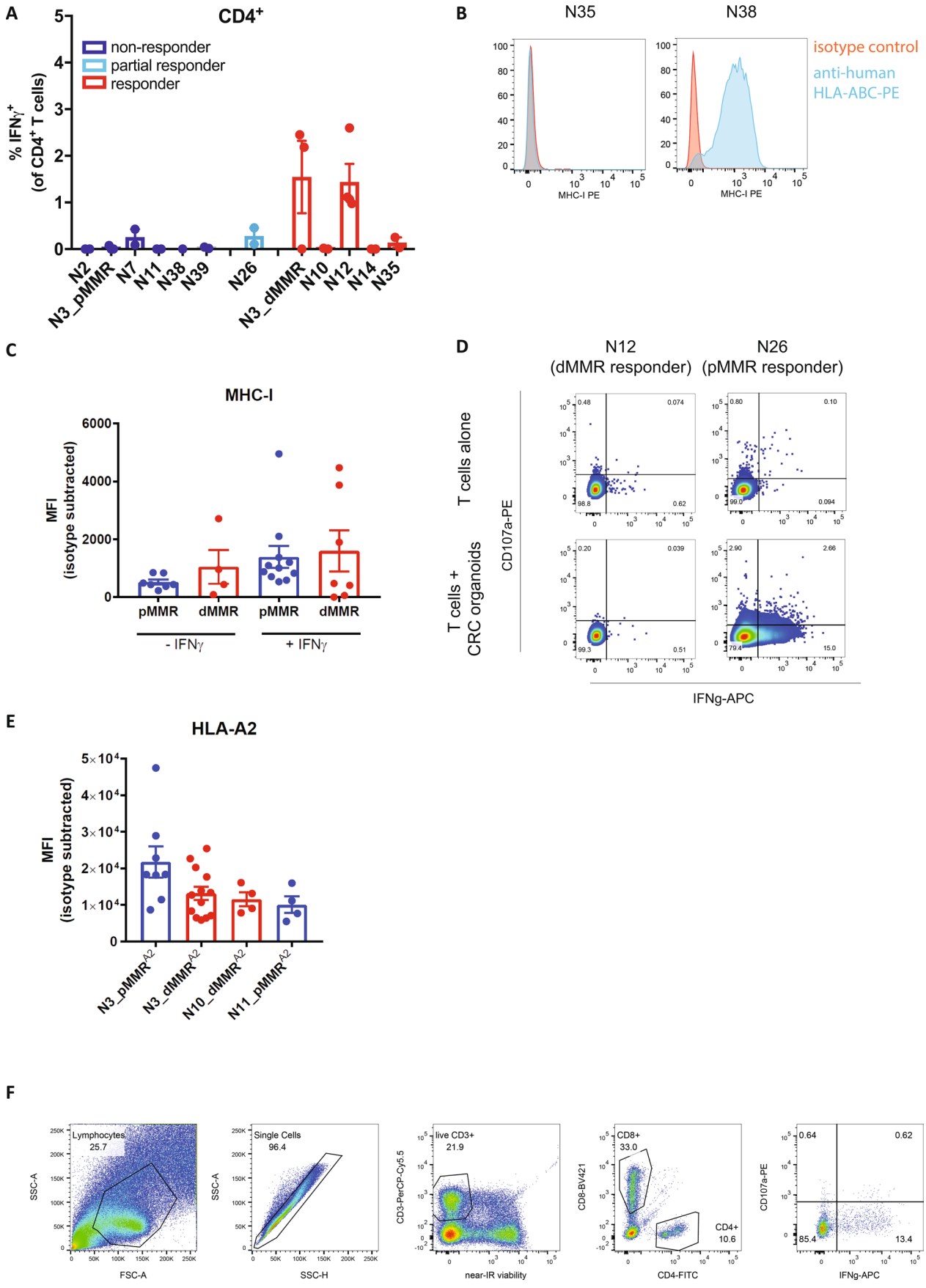

Extended Data Fig. 4 | See next page for caption.

Extended Data Fig. 4 | Organoid – T cell co-cultures. Panel **a**, Quantification of IFNγ production by CD4+ T cells, obtained by two-week co-culture with autologous tumor organoids, upon stimulation with CC organoids. pMMR non-responders are indicated in dark blue(n=6), pMMR tumor with 30% regression in light blue (n=1), dMMR responders in red (n=5). Number of biologically independent experiments: N3 (n=3); N12 (n=4); N38 (n=1); all other samples (n=2). Background (spontaneous IFNγ production) is subtracted from organoid-induced IFNγ production. Error bars reflect mean ± s.e.m. Panel **b**, Representative flow cytometry histograms of cell surface MHC-I expression of CC organoids after 24-hour pre-stimulation with 200 ng/mL IFNγ. Experiment was performed once. Panel **c**, Cell surface MHC-I expression of CC organoids with or without 24-hour pre-stimulation with 200 ng/mL IFNγ. Median fluorescence intensitity (MFI) of isotype subtracted from signal. pMMR – IFNγ (n=7); dMMR – IFNγ (n=4); pMMR + IFNγ (n=11); dMMR + IFNγ (n=7). Error bars reflect mean ± s.e.m. Panel **d**, Representative flow cytometry plots of CD8+ T cells tested for tumor reactivity, after two weeks of co-culture with autologous colon cancer (CC) organoids. Number of biologically independent experiments: N12 (n=4); N26 (n=2). Panel **e**, Quantification of cell surface HLA-A2 expression by flow cytometry of HLA-A2-transduced dMMR (n=2) and pMMR (n=2) CC organoids. Number of biologically independent experiments: N3_pMMR (n=8); N3_dMMR (n=13); N10_dMMR(n=4), N11_pMMR(n=4). Error bars reflect mean ± s.e.m. Panel **f**, Gating strategy used in tumor reactivity assays.

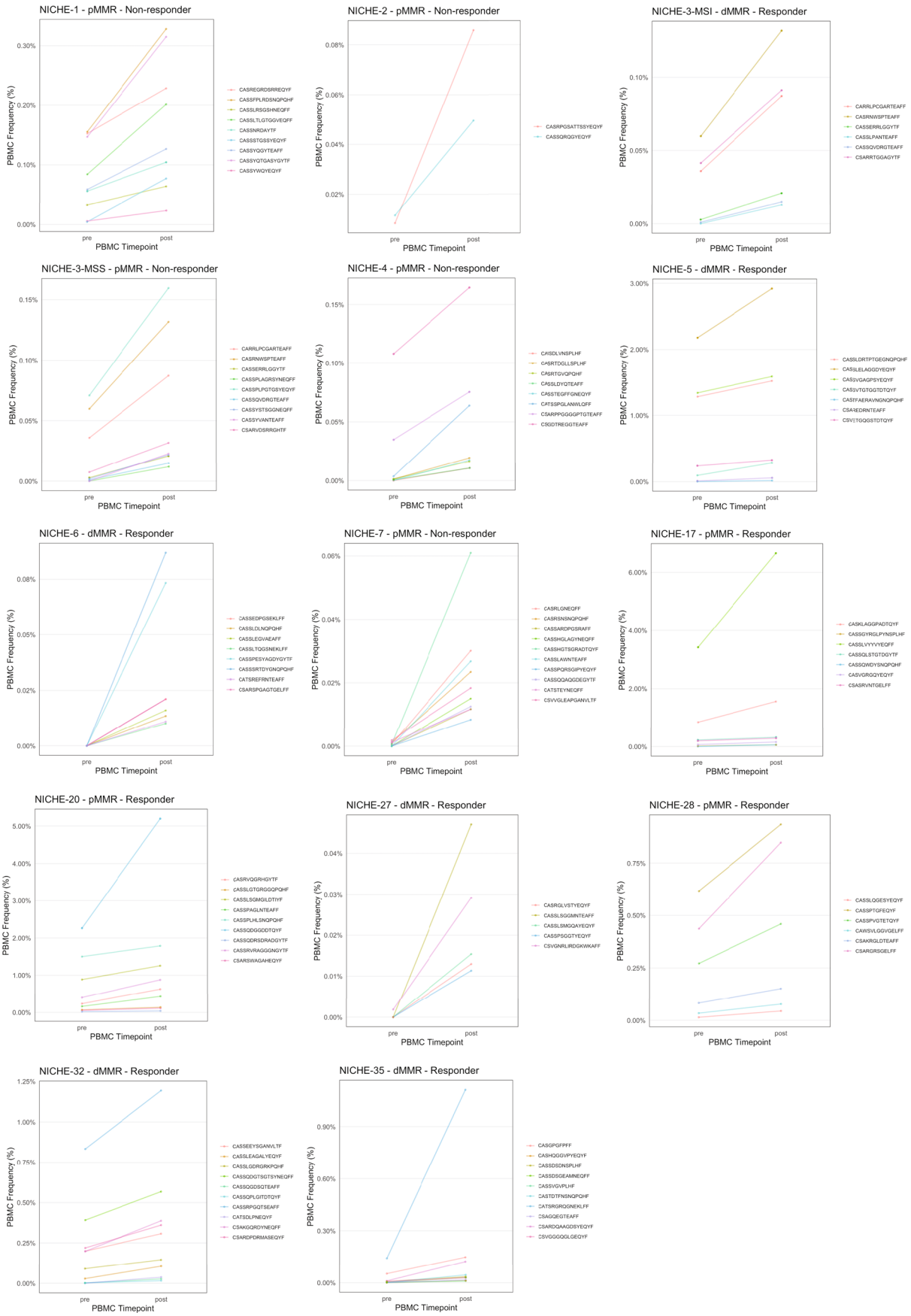

Extended Data Fig. 5 | See next page for caption.

Extended Data Fig. 5 | Peripheral expansion of intra-tumoral T cells. For 14 tumors (5 dMMR responders, 5 pMMR non-responders and 4 pMMR responders) in 13 patients, T cell receptor (TCR) sequencing was performed on pre- and post-treatment peripheral blood as well as tissue from both timepoints. Figures per patient show the top 10 most frequent intratumoral clones that undergo expansion in peripheral blood post-treatment. Data are shown as the percentage of total TCR reads. (Number of patients and tumors is not equal due to one patient with a double tumor (NICHE-3_dMMR, NICHE-3_pMMR).

nature research

Corresponding author(s): M. Chalabi, E. Voest

Last updated by author(s): Feb 1, 2020

Reporting Summary

Nature Research wishes to improve the reproducibility of the work that we publish. This form provides structure for consistency and transparency in reporting. For further information on Nature Research policies, see Authors & Referees and the Editorial Policy Checklist.

Statistics

For all statistical analyses, confirm that the following items are present in the figure legend, table legend, main text, or Methods section.

n/a	Confirmed	
☐	☒	The exact sample size (*n*) for each experimental group/condition, given as a discrete number and unit of measurement
☐	☒	A statement on whether measurements were taken from distinct samples or whether the same sample was measured repeatedly
☐	☒	The statistical test(s) used AND whether they are one- or two-sided *Only common tests should be described solely by name; describe more complex techniques in the Methods section.*
☐	☒	A description of all covariates tested
☐	☒	A description of any assumptions or corrections, such as tests of normality and adjustment for multiple comparisons
☐	☒	A full description of the statistical parameters including central tendency (e.g. means) or other basic estimates (e.g. regression coefficient) AND variation (e.g. standard deviation) or associated estimates of uncertainty (e.g. confidence intervals)
☐	☒	For null hypothesis testing, the test statistic (e.g. *F*, *t*, *r*) with confidence intervals, effect sizes, degrees of freedom and *P* value noted *Give P values as exact values whenever suitable.*
☒	☐	For Bayesian analysis, information on the choice of priors and Markov chain Monte Carlo settings
☒	☐	For hierarchical and complex designs, identification of the appropriate level for tests and full reporting of outcomes
☒	☐	Estimates of effect sizes (e.g. Cohen's *d*, Pearson's *r*), indicating how they were calculated

Our web collection on statistics for biologists contains articles on many of the points above.

Software and code

Policy information about availability of computer code

Data collection	TENALEA clinical trial data management system BD FACSDIVA (v7)
Data analysis	R version 3.5.1; BD FACSDIVA (v7); FlowJo (v10); R (v3.5.1); GraphPad Prism (v7.03); Adaptive ImmunoSEQ analyzer (v3); bwa-mem (v0.7); Picard (v2.10); GATK (v3.8.0); STAR RNAseq aligner (v2.5.3a); Salmon (v0.9.1), HALO™ image analysis software, v.2.0.1145.19 (Indica Labs, Corrales, NM), MuTect2, DESeq2 R package (Love 2014, R package version DESeq2_1.22.2, biomaRt R package (version biomaRt_2.38.0), Ensembl version 95.

For manuscripts utilizing custom algorithms or software that are central to the research but not yet described in published literature, software must be made available to editors/reviewers. We strongly encourage code deposition in a community repository (e.g. GitHub). See the Nature Research guidelines for submitting code & software for further information.

Data

Policy information about availability of data

All manuscripts must include a data availability statement. This statement should provide the following information, where applicable:

- Accession codes, unique identifiers, or web links for publicly available datasets
- A list of figures that have associated raw data
- A description of any restrictions on data availability

The RNA and DNA sequencing data will be deposited into the European Genome-phenome Archive under accession number EGAS00001004160 and will be made available on reasonable request for academic use and within the limitations of the provided informed consent. Every request will be reviewed by the institutional review board of the NKI; the researcher will need to sign a data access agreement with the NKI after approval. The TCR sequencing data that support the findings of this study are available from Adaptive Biotechnologies; however, restrictions apply to the availability of these data, which were used under license for the current study and are not publicly available. However, data are available from the authors on reasonable request and with the permission of Adaptive Biotechnologies.

Field-specific reporting

Please select the one below that is the best fit for your research. If you are not sure, read the appropriate sections before making your selection.

☒ Life sciences ☐ Behavioural & social sciences ☐ Ecological, evolutionary & environmental sciences

For a reference copy of the document with all sections, see nature.com/documents/nr-reporting-summary-flat.pdf

Life sciences study design

All studies must disclose on these points even when the disclosure is negative.

Sample size	Safety and feasibility were evaluated after the first three patients in the run-in period had undergone surgery and were released from hospital, and the local ethics board approved further accrual. This procedure was repeated after a total of 6 patients had been included. After establishing safety and feasibility in the first six patients according to the primary endpoint, accrual was continued into an exploratory expansion cohort. For this exploratory, hypothesis-generating study, no formal sample size calculation was performed for efficacy, since there were no data on neoadjuvant immunotherapy and the expected effect size in colon cancer. Based on the expected accrual of patients in a period of two years, the study aimed to include 60 patients total, of which 30 with pMMR tumors and 30 with dMMR tumors (Extended Data Fig.1). The NICHE study is currently still enrolling and based on emerging results can be adapted to included other treatment combinations and expand cohorts accordingly.
Data exclusions	All patients were included for safety analyses. In the translational data analyses patients who received nivolumab monotherapy (n=3) and patients who were ineligible for the study (n=2) were excluded from translational analyses. Organoids were authenticated by SNParray and regularly tested for Mycoplasma using mycoplasma PCR and the MycoAlert Mycoplasma Detection Kit (Lonza, ref. LT07-318).). Organoids that could not be authenticated or were Mycoplasma contaminated were excluded from analysis.
Replication	All our work is replicable. For organoid experiments, we have documented in detail the source of materials used as well as the experimental procedure in the Methods section. We have also recently published a detailed protocol of organoid – T cell co-cultures in a sister journal, Nature Protocols (Cattaneo, C.M., et al. Tumor organoid-T-cell coculture systems. Nat Protoc 15, 15-39 (2020).). We have referred to this detailed protocol in this manuscript.
Randomization	Patients received ipilimumab 1mg/kg on day (D)1 and nivolumab 3mg/kg on D1+D15. In addition, patients with pMMR tumors were randomized between ipilimumab/nivolumab plus celecoxib 200mg daily, or ipilimumab/nivolumab without celecoxib.
Blinding	Since all patients were allocated to receive ipilimumab plus nivolumab, blinding was not performed.

Reporting for specific materials, systems and methods

We require information from authors about some types of materials, experimental systems and methods used in many studies. Here, indicate whether each material, system or method listed is relevant to your study. If you are not sure if a list item applies to your research, read the appropriate section before selecting a response.

Materials & experimental systems

n/a	Involved in the study
☐	☒ Antibodies
☒	☐ Eukaryotic cell lines
☒	☐ Palaeontology
☒	☐ Animals and other organisms
☐	☒ Human research participants
☐	☒ Clinical data

Methods

n/a	Involved in the study
☒	☐ ChIP-seq
☐	☒ Flow cytometry
☒	☐ MRI-based neuroimaging

Antibodies

Antibodies used

- MLH1 Ready-to-Use, M1, 6472966001, LotNo: G07286, Roche, Basel, Switzerland
- MSH2, Ready-to-Use, G219-1129, 5269270001, LotNo: 1616008C, Roche, Basel, Switzerland
- MSH6, 1/50 dilution, EP49, AC-0047, LotNo: EN020910, Abcam, Cambridge, United Kingdom
- PMS2,1/40 Dilution, EP51, M3647, LotNo: 1012289 Agilent Technologies, Santa Clara, CA
- CD3 clone clone SP7, 1/100 dilution for 32 minutes at 37 degrees C, LotNo: 160407LVP, Spring / ITK
- CD8 clone C8/144B CA1/200 dilution, LotNo: 20066516, DAKO/Agilent Technologies, Santa Clara, CA
- FOXP3 clone 236A/E7 1/200 dilution for 2 hours at RT, LotNo: GR3220121-1, AbCam, Cambridge, United Kingdom
- CD20 clone L26 1/800 dilution, for 32 minutes at 37 degrees C, LotNo: 20038880, DAKO/Agilent Technologies, Santa Clara, CA
- CD68 clone KP1, 1/10000 dilution for 32 minutes at 37 degrees C, LotNo:20040389, DAKO/Agilent Technologies, Santa Clara, CA
- PD1 clone NAT105 Ready-to-Use, for 16 minutes at RT, LotNo: V0001234, Cell Marque / Roche

- PDL1 clone 22C3 1:40 dilution for 1 hour RT, LotNo: 10137461, DAKO / Agilent Technologies, Santa Clara, CA

Organoid experiments:
• Mouse anti-human CD28 (eBioscience,CD28.2, 1/200 dilution, cat. no. 16-0289-81)
• Mouse anti-human CD107a (PE-conjugated) (1/100 dilution, BD, clone H4A3, cat. no. 555801)
• Mouse anti-human CD3 (PerCP-Cy5.5-conjugated) (eBioscience, clone SK7, 1/20 dilution, cat. no. 332771)
• Mouse anti-human CD4 (FITC-conjugated) (BD, clone RPA-T4, 1/20 dilution, cat. no. 555346)
• Mouse anti-human CD8 (BV421-conjugated) (BD, clone RPA-T8, 1/200 dilution, cat. no. 562429)
• Mouse anti-human IFNγ (APC-conjugated) (BD, clone B27, 1/40 dilution, cat. no. 554702)
• Mouse anti-human HLA-A2 (APC-conjugated, BD, clone B97.2, 1/20 dilution, cat. no. 561341)

Validation

Each IHC protocol has been developed and validated in diagnostic setting under standard operating procedures in a certified pathology lab (EN ISO15189, M258).
Each new antibody lot is validated by testing multiple dilutions and evaluating them with the pathologist in a standardized method, using positive control tissues suitable for the antibody (images and protocol details available upon request).

Validation of antibodies used in organoid experiments: Mouse anti-human CD28: Validated for flow cytometry on normal human peripheral blood cells by manufacturer. Mouse anti-human CD107a: Validated and routinely tested for flow cytometry on Jurkat cells and activated platelets by manufacturer. Mouse anti-human CD3: Routinely tested for flow cytometry on human thymocytes by manufacturer. Mouse anti-human CD4: Validated and routinely tested for flow cytometry on human peripheral blood lymphocytes by manufacturer. Mouse anti-human CD8: Validated for flow cytometry on human peripheral blood lymphocytes by manufacturer. Mouse anti-human IFNγ: Validated for flow cytometry on human peripheral blood mononuclear cells by manufacturer. Mouse anti-human HLA-A2: Validated for flow cytometry on human peripheral blood lymphocytes by manufacturer.

Human research participants

Policy information about studies involving human research participants

Population characteristics	Eligible patients were 18 years and older and had stage I, II or III resectable colon adenocarcinoma. All patients had an Eastern Cooperative Oncology Group performance-status score of 0 or 1 and adequate end-organ function. Key exclusion criteria were clinical signs of bowel obstruction, immunosuppressive treatment, immunodeficiency, active autoimmune disease and active other cancer.
Recruitment	Patients either presented at our center with initial diagnosis of colon cancer, or were referred from other centers, mainly the OLVG. All patients who were deemed eligible for the study were informed.
Ethics oversight	The study protocol was approved by the local ethics board of the NKI (sponsor) and was conducted in accordance with the ICH Harmonized Tripartite Guideline for Good Clinical Practice and the principles of the Declaration of Helsinki. All patients provided written informed consent.

Note that full information on the approval of the study protocol must also be provided in the manuscript.

Clinical data

Policy information about clinical studies

All manuscripts should comply with the ICMJE guidelines for publication of clinical research and a completed CONSORT checklist must be included with all submissions.

Clinical trial registration	ClinicalTrials.gov NCT03026140
Study protocol	The study protocol will be made available upon request and will be uploaded together with initial submission of the manuscript.
Data collection	Clinical data was collected from the time of informed consent up until 100 days after the last administration of nivolumab. Outcome data and long-term survival will be collected until five years after initial diagnosis. The first patient was enrolled on the 29th of March 2017. Data collection for the current analysis was performed on the 21st of October 2019. eCRF database is located at The Netherlands Cancer Institute, Amsterdam, NL.
Outcomes	Primary objectives were safety and feasibility. All patients were closely monitored for adverse events (AEs) until 100 days after the administration of the last nivolumab dose, according to the Common Terminology Criteria for Adverse Events CTCAE 4.03.33 The most severe toxicity grade over all cycles according to the CTCAE criteria version 4.03 was depicted by body system. Safety was assessed by evaluation of AEs and serious AE (SAEs) and feasibility was determined based on any treatment-related complications leading to delays in surgery past the 6 weeks after informed consent, or unexpected post-surgery complications. Safety and feasibility were evaluated after the first three patients in the run-in period had undergone surgery and were released from hospital, and the local ethics board approved further accrual. This procedure was repeated after a total of 6 patients had been included. After establishing safety and feasibility in the first six patients according to the primary endpoint, accrual was continued into an exploratory expansion cohort. Secondary and translational endpoints included efficacy, as assessed by histopathological response to treatment, and associations between response and immunological, morphological and genomic findings, including tumor mutational burden (TMB), interferon (IFNγ) gene signatures, T-cell infiltration (TCI) and T-cell receptor (TCR) clonality.

Flow Cytometry

Plots

Confirm that:

☒ The axis labels state the marker and fluorochrome used (e.g. CD4-FITC).

☒ The axis scales are clearly visible. Include numbers along axes only for bottom left plot of group (a 'group' is an analysis of identical markers).

☒ All plots are contour plots with outliers or pseudocolor plots.

☒ A numerical value for number of cells or percentage (with statistics) is provided.

Methodology

Sample preparation	Patient T cells were co-cultured with organoids for 2 weeks and collected for analysis
Instrument	Beckton Dickinson Fortessa I
Software	FacsDiva v8.0.2
Cell population abundance	Organoids expressing HLA-A2 after transduction were FACS-sorted. Purity was evaluated using flow cytometry and was >98%".
Gating strategy	For Figure 5a, 5d and S4d: FSCxSSC gated on live lymphocytes -->> SSC-H x SSC-A gated on single cells -->> CD3-PerCP-Cy5.5 x near-IR viability gated on live CD3+ cells -->> CD4-FITC x CD8-BV421 gated on CD4+ or CD8+ cells -->> IFNg-APC x CD107a-PE: quadrant gate separating single positive, double positive and double negative cells.

☒ Tick this box to confirm that a figure exemplifying the gating strategy is provided in the Supplementary Information.